Journal of Materials Processing Technology 231 (2016) 336–356

Contents lists available at ScienceDirect

Journal of Materials Processing Technology

journal homepage: www.elsevier.com/locate/jmatprotec

The ultra-precision U_d-lap grinding of flat advanced ceramics

Arthur Alves Fiocchi [a,*], Luiz Eduardo de Angelo Sanchez [b], Paulo Noronha Lisboa-Filho [c], Carlos Alberto Fortulan [a]

[a] University of São Paulo—USP, Department of Mechanical Engineering, Av. Trabalhador Saocarlense 400, 13566-590 São Carlos, SP, Brazil
[b] São Paulo State University—Unesp, Department of Mechanical Engineering, Av. Luiz Edmundo Carrijo Coube, 14-01, 17033-360, Bauru, SP, Brazil
[c] São Paulo State University—Unesp, Department of Physics, Av. Luiz Edmundo Carrijo Coube 14-01, 17033-360, Bauru, SP, Brazil

ARTICLE INFO

Article history:
Received 10 April 2015
Received in revised form 1 October 2015
Accepted 4 October 2015
Available online 23 October 2015

Keywords:
U_d-lap grinding
Advanced ceramics
Ductile grinding
Surface characterization
Nanotechnology

ABSTRACT

The present study focuses on the U_d-lap grinding process and its machine-tool design aiming at ultra-precision (UP) manufacturing of advanced ceramics. Impacts of three different overlapping factors on a dressing (U_d) and three abrasive grit sizes of conventional SiC grinding wheels were analyzed on flat nanometric surface finishing of dense discs of 3Y-TZP in a ductile regime of material removal. Microhardness, contact and optical profilometry, SEM-FEG, Raman spectroscopy, XRD, and confocal epi-fluorescence were applied to characterize the ceramic material. Mechanical and electric-electronic designs of the machine-tool were developed toward the UP ceramic grinding. The design methodology was successful for supporting the achievement of all design requirements of the CNC Fiocchi Lap Grinder. The machine-tool and the U_d-lap grinding process were capable of manufacturing flat 3Y-TZP surfaces with nanometric finishing without introducing critical defects. The best finishing, Ra = 60.63 nm, came from the #300 grinding wheel dressed with U_d = 5. A flatness deviation of 0.308 μm was obtained through the #800 grinding wheel and U_d = 3. Differences between theoretical and real macro and micro effects over the grinding wheels after single-point diamond dressing, epoxy bond strength, abrasive protrusion, abrasive grit size and abrasive friability play a key role in the U_d-lap grinding. There is no report of an abrasive process capable of achieving similar nanometric finishing without introducing critical defects with the same micrometric grit size and type of abrasive. The U_d-lap grinding can replace the engagement of processes such as grinding, lapping, and polishing of advanced ceramics.

1. Introduction

Compared with metals, advanced ceramics are materials of higher hardness and special properties that present performance, reliability, and safety at elevated temperatures; these are outcomes of their exceptional chemical stability due to strong ionic and/or covalent atomic bonds (Boch and Nièpce, 2007). However, advanced ceramics suffer from their relatively low fracture toughness, which also significantly affects their cost as a result of post-sintering processing normally done by expensive superabrasive tools and manufacturing processes (Janssen et al., 2008).

Except for glass, plastic molding and casting of advanced ceramics are exceptionally high cost, mainly because of the chemical bonds that raise the melting point. Brittleness is also a significant characteristic of these ceramics below 1000 °C. In addition to limiting their use, the brittleness imposes restrictions on production techniques. All these limitations of ceramic manufacturing explain why the basic technique of densification is the sintering of compacted powder (Boch and Nièpce, 2007). This opposition is quite evident between metals (ductile) and ceramics (fragile).

As ceramics are more brittle, the main mechanical failure usually occurs by crack propagation (Argawal and Rao, 2008). Initial critical cracks, precursors of the failure, are defects usually originating in irregularities acquired in the early stages of obtaining the piece (from powder to sintering) (Bukvic et al., 2012) and/or during its post-sintering processing (hard ceramic machining) (Marinescu et al., 2014), hence the design of a product of advanced ceramic needs special care in each phase of its manufacturing.

In general lines, in the production of a ceramic artifact, the raw materials (powders) are milled or synthesized, are mixed, and receive additives such as binders and plasticizers to assist the conformation, compaction, and sintering (Scheller, 1994). The ceramic powder is formed into compacted pieces, also called green parts due to their not heat treated state, which are subsequently sintered to

* Corresponding author.
E-mail addresses: arthuraf@eesc.usp.br (A.A. Fiocchi), sanchez@feb.unesp.br (L.E. de Angelo Sanchez), plisboa@fc.unesp.br (P.N. Lisboa-Filho), cfortula@sc.usp.br (C.A. Fortulan).

http://dx.doi.org/10.1016/j.jmatprotec.2015.10.003
0924-0136/

Nomenclature

a_d	Depth of dressing (mm)
AE	Acoustic emission
AISI	American Iron and Steel Institute
ASTM	American Society for Testing and Materials
b_d	Dressing width
CNC	Computer numerical control
Cps	Counts per second
E	Elastic modulus (GPa)
EESC	São Carlos School of Engineering
ELID	Electrolytic-in process dressing
FAPESP	São Paulo Research Foundation
FEB	Bauru College of Engineering
HFW	Horizontal field width (mm)
HV	Hardness vickers
HV	High voltage (kV)
IFSC	São Carlos Institute of Physics
k	Parameter for monoclinic phase quantification by Raman spectroscopy
K_{IC}	Fracture toughness (MPa.m$^{0.5}$)
LATUS	Laboratory of Machining Technology
l_n	Total measured length (mm)
LTC	Laboratory of Tribology and Composite
l_r	Single measured length (mm)
m	Monoclinic phase
MEMS	Micro-electromechanical systems
m_f	Final mass (g)
m_i	Initial mass (g)
MQF	Minimum quantity fluid
MRR	Material removal rate (g/minute)
NEMS	Nano-electromechanical systems
n_g	Grinding wheel rotational speed (rpm)
n_w	Workpiece rotational speed (rpm)
P	U_d-lap grinding pressure (kPa)
PABA	4-Aminobenzoic acid
PVB	Polyvinyl-butyral
PVD	Physical vapor deposition
Ra	Arithmetic mean surface roughness (μm)
RMS	Root mean square
r_p	Dresser nose radius geometry (mm)
Rt	Total height of the roughness profile (μm)
r	Stylus tip radius (μm)
Sa	Arithmetic mean height over the complete 3D surface (μm)
S_d	Dressing feed
SE	Secondary electron detection
SEM-FEG	Scanning electron microscope equipped with field emission gun
SiC	Silicon carbide
Sku	Kurtosis of the 3D surface texture
Sp	Max peak height over the complete 3D surface (μm)
Sq	Root mean square height evaluated over the complete 3D surface (μm)
Ssk	Skewness of the 3D surface texture
Sv	Maximum valley depth over the complete 3D surface (μm)
Sz	Maximum height over the complete 3D surface (μm)
T	Tetragonal phase
TZ-3Y-E	Tosoh zirconia grade
$t \rightarrow m$	Martensitic transformation
U_d	Overlap factor or overlap ratio on dressing
UNESP	Universidade Estadual Paulista
UP	Ultra-precision
USP	University of São Paulo
V_{crit}	Critical velocity of the jar
V_m	Volume of monoclinic phase (%)
V_m max	Maximum volume of monoclinic phase (%)
V_m min	Minimum volume of monoclinic phase (%)
XRD	X-ray diffraction
WD	Working distance (mm)
W	Real waviness (μm)
Y-TZP	Tetragonal zirconia polycrystals stabilized with yttria
ZrO_2	Zirconium oxide or zirconia
3Y-TZP	Tetragonal zirconia polycrystals stabilized with 3 mol% of yttria
α	Single abrasive relief angle (°)
β	Single abrasive wedge angle (°)
γ	Single abrasive rake angle (°)
δ	Parameter for monoclinic phase quantification by Raman spectroscopy
θ	Diffraction angle (°)
λ_c	Cutoff (mm)
ρ	Density (g/cm^3)
σ	Bending strength (MPa)
Ø	Diameter (mm)
#	Mesh number of the grinding wheel (abrasive grit size)

achieve the desired hardness and density (Richerson, 2006). Each step has the potential to produce undesirable microstructural flaws in the piece, which in itself may limit their properties, reliability, and machinability. Scientific investigations are not exclusively focused on the material itself, but also in its processing into powder, granules, and in the subsequent stages of obtaining a part as well as its machining.

For less demanding applications regarding form and finish, the sintering is the last stage of the ceramic processing. Nevertheless, several areas of science and technological applications require better finishing, tighter dimensional and geometric tolerances, and surfaces completely free of damage (Brinksmeier et al., 2010). Such parts must undergo, consequently, further processing steps after sintering, especially to confer on them complex geometries and finer finishing. The demands for better surface finishing and high accuracy of optical, electrical, and mechanical components are growing along with the miniaturization of high performance products, such as lenses, electronic components of computers and smartphones, and sensors, as well as micro and nano-electromechanical systems (MEMS and NEMS).

Among the available methods of material removal, the abrasive machining is the most widespread in industry. Grinding reconciles stock removal, form correction, and surface quality for large-scale production in an economically feasible way (Malkin, 1989). Although widespread, hard ceramic machining is an extremely difficult task due to the exceptional ceramic properties in the sintered state, especially: high hardness, high elastic modulus, high melting point, and fragility (Callister and Rethwisch, 2013). These require superabrasive cutting tools, stiff machine-tools and clamping devices, micro and nanometer depths of cut, and a highly skilled workforce (Brinksmeier et al., 2010).

In traditional abrasive technology, the brittle mode is the primary removal mechanism (Marinescu et al., 2004) caused by the propagation of lateral cracks that promote chipping (Xu and Jahanmir, 1995). Higher removal rates can be achieved in the brittle mode in opposition to ductile abrasive cutting (Xu et al., 1995). On

the other hand, grinding may also generate longitudinal cracks that can remain in the product after grinding (Marinescu et al., 2007) and act, for example, as stress concentrators that under specific conditions stimulate subcritical crack propagation (Deville et al., 2006).

The main technological challenge of hard ceramic machining is, thus, to promote material removal without introducing critical defects that will compromise the performance of the component (Marinescu et al., 2014). Therefore, the brittle removal mode should be avoided in ultra-precision (UP) grinding or minimized in order to avoid mainly the formation and propagation of surface and subsurface cracks, microstructural changes, and residual tensile stress (Brinksmeier et al., 2010).

To minimize the emergence and evolution of cracks, machining should be conducted with discretion, so as to avoid the introduction of residual tensile stress on surfaces of materials subject to stress-induced phase transformation (Deville et al., 2006). The search for high-tech ceramic parts with functional surfaces requires, hence, the most sophisticated manufacturing processes.

Over the last three decades, researchers have responded to demands of industry for machine-tools and fabrication processes that aim to attain high-precision parts in a nanometer (10^{-9} m) and angstrom (10^{-10} m) for both dimensional and finish range (Ohmori, 2011). Nevertheless, these quality characteristics are very difficult, or economically unviable, to achieve by concatenating the traditional abrasive processes such as grinding, lapping, and polishing.

For finishing flat surfaces, researchers have been putting together the main advantages of the traditional abrasive processes such as: face grinding with constant pressure, fixed abrasives for a two-body removal mechanism, total contact of the part with the tool, and lapping kinematics as well as some specific operations to keep grinding wheel sharpness and form. In this way, different dressing and conditioning techniques have been applied to the tool before and/or during grinding processes. According to Sanchez et al. (2011), these different dressing procedures yield distinguished results in grinding performance. Nanogrinding (Gatzen and Maetzig, 1997), face grinding with lapping kinematics or grinding on a lapping machine (Tomita and Eda, 1996), ELID-lap grinding (Ohmori et al., 2011), flat honing (Beyer and Ravenzwaaij, 2005), and U_d-lap grinding (Fiocchi et al., 2015) are some examples of these high-end grinding processes for finishing flat surfaces.

The Brazilian process, named U_d-lap grinding, was created to meet the demands for a gold-standard abrasive processes as an economical and accessible technique for industry, especially the Brazilian one, which until now employed only foreign technologies for UP finishing of flat advanced materials (Fiocchi et al., 2015).

U_d-lap grinding investigations started with an adapted lapping machine (Sanchez et al., 2011). Fiocchi Lap Grinder I (Fiocchi, 2010 Fiocchi et al., 2015) came next to establish the first fully CNC machine-tool to grind flat metallic surfaces using epoxy bonded SiC grinding wheels dressed according to the overlap factor theory (U_d) proposed by König and Messer (1980). The second version (Fiocchi, 2014), presented in this paper, represents a cutting-edge CNC machine-tool design, improved for grinding materials that are not only ductile, but also hard and difficult to machine.

Products made of tetragonal zirconia polycrystals stabilized with yttria (Y-TZP) have a noticeable interest in functional surfaces that require top-quality mechanical (Zhuang et al., 2015), electrical (Flegler et al., 2014), and tribological properties (Chevalier et al., 2007).

The 3Y-TZP used under some specific conditions presents a complex phenomenon of subcritical crack growth defined, among other names, as stress corrosion (Sikalidis, 2011) or low temperature degradation (LTD) (Chevalier et al., 2007). This mechanism promotes the change of the crystalline structure from tetragonal to monoclinic ($t \rightarrow m$) when the ceramic is subjected to stress and/or temperature (Kelly and Rose, 2002), especially in the presence of water (Yoshimura et al., 1987). This structural change of a martensitic nature generates volumetric expansion of the monoclinic phase (Kelly and Rose, 2002) that generates cracks and stimulates their propagation (Schmauder and Schubert, 1986), therefore influencing the mechanism of material removal.

There is concern that 3Y-TZP products suffer unwanted phase destabilization under undersized conditions, even without applying stress (Li et al., 2001). Under circumstances of external loading during either the manufacture or use of the ceramic product, this destabilization can happen. In this context, the transformation can be triggered by temperatures and stresses from the machining process (Deville et al., 2006). The presence of aqueous-based cutting fluid can accentuate this phenomenon of phase destabilization.

The microstructural control capability of this event makes the 3Y-TZP a key material in the evaluation of UP machining processes, allowing its scientific study by qualifying and quantifying the martensitic transformation induced by chip removal.

The present work has as its hypothesis the possibility that the achievement of flat surfaces with nanometric finishing ($Ra < 100$ nm) in advanced ceramics without critical defects is possible by combining appropriate machine-tool kinematics and grinding pressure, proper cutting tool sharpening, and specific lubrication and cooling.

To prove this hypothesis, the Fiocchi Lap Grinder's design was evolved, aiming at UP face grinding with lapping kinematics of advanced ceramics, meeting the conditions of removal and finishing in a single automated process and equipment.

The 3Y-TZP was chosen as the workpieces' material due to its phase transformation under severe removal conditions, for instance, excessive specific cutting pressure and high temperatures in a humid atmosphere. Grinding wheels made of silicon carbide (SiC) grits and epoxy bond were applied under different U_d dressing parameters and water as a dressing fluid.

2. Experimental set-up

2.1. Machine-tool

A second version of the Fiocchi Lap Grinder was used in this work, named Fiocchi CNC Lap Grinder II. The machine-tool was conceptualized and designed in a partnership between the Laboratory of Tribology and Composite (LTC) at Escola de Engenharia de São Carlos (EESC) of Universidade de São Paulo (USP), São Carlos Campus, and the Laboratory of Machining Technology (LATUS) at Faculdade de Engenharia de Bauru (FEB) of Universidade Estadual Paulista (UNESP), Bauru campus. The machine-tool was put together and validated at LATUS. As well as being applied to build the first Fiocchi's machine-tool during his Master's course (Fiocchi, 2010), design methodology (Pahl et al., 2007) was used to evolve Lap Grinder I, aiming the ultra-precision (UP) manufacturing of advanced ceramics by improving critical aspects pointed out in early studies of Sanchez et al. (2011), Fiocchi (2010), and Fiocchi et al. (2015).

Fig. 1 compares some of the modifications implemented in Fiocchi Lap Grinders. The main improvements from Lap Grinder I (Fig. 1a) (Fiocchi, 2010; Fiocchi et al., 2011) to Lap Grinder II (Fig. 1b) (Fiocchi, 2014) were: (1) substitution of the flexible shaft by a servomotor to control a workpiece's angular velocity; (2) a new spindle having two tapered roller bearings mounted in a back-to-back configuration, 50 N pre-load, and a hollow shaft for supporting a vacuum chuck, which has a universal joint with two degrees-of-freedom to keep workpiece's surface parallel to the grinding wheel; (3) new stepping motors and drives to prevent linear axis resonating; (4) new physical configuration of the novel electrical

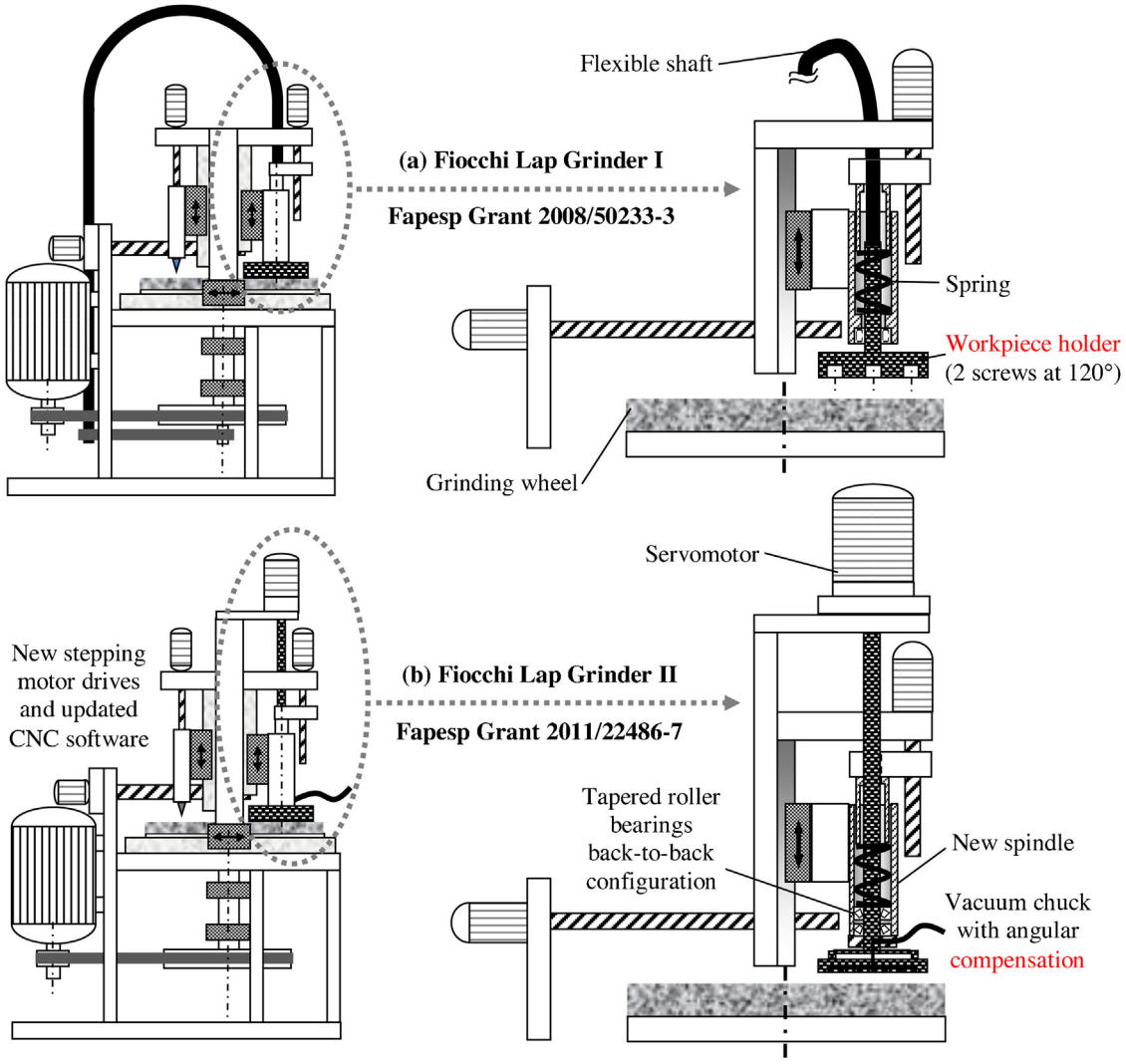

Fig. 1. (a) Fiocchi Lap Grinder I, (b) Fiocchi Lap Grinder II.

components inside the main electrical panel; and (5) updated software and grinding strategy to improve linear axis dynamics.

2.2. Workpiece material

Zirconia powder with 3 mol% of yttria (Y_2O_3) from Tosoh (TZ-3Y-E) was chosen as the raw ceramic material due to its attractive surface and mechanical (strength and toughness) properties after sintering in the present study. Moreover, tetragonal zirconia policristal stabilized with 3 mol% of yttria (3Y-TZP) is a key material for medical and dental implants as well as the electronic and mechanical industries. According to Tosoh, after sintering, 3Y-TZP can achieve hardness of 1250 HV, elastic modulus (E) of 210 GPa, bending strength (σ) of 1200 MPa, fracture toughness (K_{IC}) of 5.0 MPa.$m^{0.5}$, and microstructure endowed by fine grains under 0.3 μm average diameter.

The material also presents interesting surface finishing aptitude as well as the possibility that phase transformation can be investigated in outside layers induced by grinding conditions. The occurrence and magnitude of the martensitic transformation (tetragonal → monoclinic) can, therefore, be used as a scientific tool for evaluating the quality of the material removal process.

In UP manufacturing of advanced materials, all production steps are important and have influence not only on the final mechanical and electrical properties for example, but also on surface finishing. Considering that fired advanced ceramics are hard materials that are difficult to machine, and their machining is expensive, an optimized manufacturing route should consider a near-net-shape production, in which material removal processes are used for improving mainly surface finishing.

For the best machining results, the material properties and geometry must be well-defined and controlled. In the present research, hence, it was pre-defined that workpieces' manufacturing route should start with TZ-3Y-E powder and aim to accomplish sintered flat ceramic discs with: (1) quasi-zero defects, (2) homogenous grain size up to 0.4 μm average diameter, and (3) dense bodies, so that U_d-lap grinding could focus on (4) achieving surface roughness (Ra) under 100 nm, removing little material using silicon carbide (SiC) grinding wheels. Fig. 2 illustrates the main steps and their parameters for manufacturing and characterization of the ceramic material from powder to U_d-lap ground discs.

2.2.1. Mixing

The powder was prepared in a ball mill with a nylon jar of 100 ml internal volume (Carvalho and Fortulan, 2006 Carvalho, 2007) rotating at 104 rpm, corresponding to 65% of the critical velocity ($V_{crit} = 1338.2/D^{0.5}$) for a 70-mm inner diameter jar (D). 30 vol% of the useful volume of the jar were filled up with TZ-3Y-

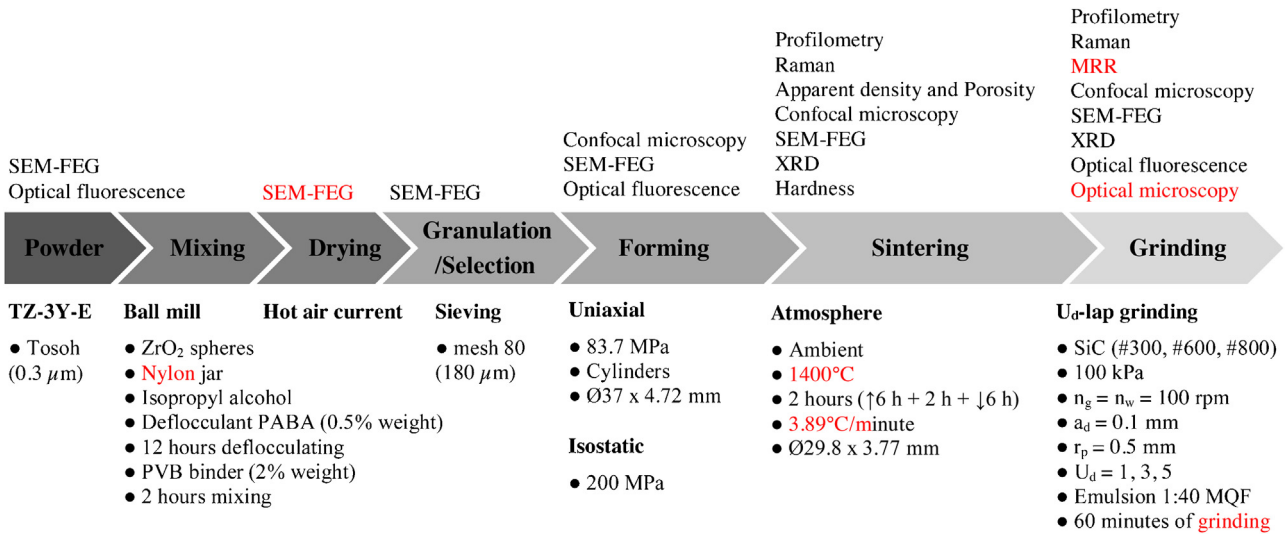

Fig. 2. Main steps and characteristics of TZ-3Y-E manufacturing and characterization.

E ($\rho = 6.05\ g/cm^3$), with 0.5 kg of milling media (Tosoh YTZ 10 mm diameter), and 70 vol% of the useful volume filled up with isopropyl alcohol ($\rho = 0.786\ g/cm^3$) as a slurry solvent. 4-Aminobenzoic acid (PABA; $\rho = 1.37\ g/cm^3$) was added in as a deflocculant in the ratio of 0.5% of the TZ-3Y-E mass. Then, the ball mill operated for 12 h. After deflocculating completed, Polyvinyl-butyral (PVB-butvar B98; $\rho = 1.1\ g/cm^3$) was added to the slurry as a binder in the ratio of 2.0% of the TZ-3Y-E mass, and the mixing continued for 2 more hours for homogenizing the colloidal suspension.

2.2.2. Drying

After the deagglomeration and mixing steps, drying was manually done by agitating the slurry in a hot air current inside a clean chamber. Gloves without talc were used and extreme care was taken in order to avoid any contamination.

2.2.3. Granulation and selection

Manual granulation and selection applied an 80-mesh (180-μm aperture) stainless steel sieve with the purpose of standardizing the agglomerate size in preparation for pressing. Granulation and selection were also performed inside the clean chamber while wearing gloves.

2.2.4. Forming

Forming took place in two steps; 13.6 g of the zirconia granules were manually inserted into the cylindrical mold with the help of a plastic container, leveled with a stainless steel spatula, and gently agitated by a vibrating table Labortechnik GmbH (THYR2 model), seeking homogenization of the filling. Next, single-acting uniaxial press happened at 83.7 MPa during 10 s in a 37-mm diameter mold to shape discs with 4.72 ± 0.03-mm thickness. Subsequent wet-bag isostatic pressing occurred in an AIP wet-bag presser (CP360 model) at 200 MPa for 30 s to homogenize the green ceramic bodies, reducing density gradients and increasing densification.

2.2.5. Sintering

Sintering occurred in an ambient atmosphere Lindberg furnace (Blue M model) with 3.89 °C/min heating and cooling rates and 2 h at 1400 °C, resulting in ceramic discs of 3.77 ± 0.02-mm thickness and 29.8 ± 0.15-mm diameter.

2.3. Ceramic characterization

According to Fig. 3, several characterization techniques were applied in this research. Apparent density and porosity were determined by ASTM C73. TZ-3Y-E powder, granules, and green and sintered workpieces' microstructure were investigated by SEM-FEG. Green, sintered, and U_d-lap ground workpieces were investigated by confocal microscopy. Optical fluorescence microscopy was applied to the powder, green body, and U_d-lap ground workpieces. Hardness Vickers were measured in sintered pieces. XRD was measured in powder, sintered and U_d-lap ground workpieces. Raman spectroscopy and profilometry were used with sintered and U_d-lap ground parts as well as optical microscopy in grinding wheels' active surface after dressing and U_d-lap grinding.

SEM applied an FEI electronic microscopy (Inspect F50 model) equipped with a field emission gun (FEG), 10 kV electron acceleration voltage, working distance between 6.7 and 10.3 mm, and secondary electron detection (SE). Above each SEM image there is a legend with the main information and conditions applied, from the left to right side: date and time, dwell time, high voltage (HV), horizontal field width (HFW), working distance (WD), detection mode, and scale. The specimens received a thin layer of gold by physical vapor deposition (PVD).

A Nikon microscope (model Eclipse TS100) and NIS Elements software were used to analyze optical fluorescence. Powder visualization applied 10× lenses and sintered pieces with 4× objective and 10× ocular lenses.

XRD was studied through a PANalytical Diffractometer (X'Pert Pro MRD model) of CoKα radiation (1.78 Å, 40 kV, and 40 mA), continued scanning, 0.02 angular resolution, 6.667×10^{-3} degrees, and 2θ ranging from 20° to 65°. Quantification of the volume percentage of the monoclinic phase was accomplished according to the models described by Toraya et al. (1984a,b) and Sato et al. (2008).

Vickers hardness was evaluated by a Mitutoyo Microhardness tester (HM-200 model) with pyramidal diamond indentator with 1 kg load for 10 s, and equal loading and unloading time of 4 s in sintered workpieces.

Raman spectrum measurements were done in a Witec Raman Confocal Microscope (Alpha 300 A/R model), Witec Control software, He-Ne laser (632 nm), and UHTS spectrum analyzer. Different points of each workpiece surface were focused on with a 1-μm diameter laser beam during 3 s of integrating time and the average result of 10 integrations was taken. Quantification of the volume

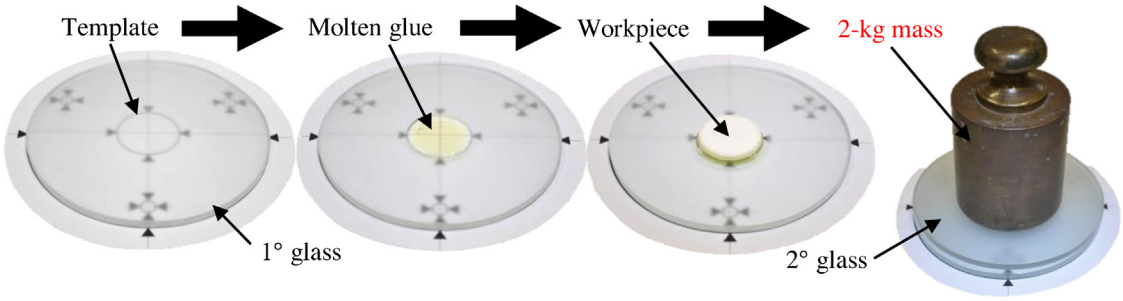

Fig. 3. Workpiece fixturing technique.

percentage of monoclinic phase was accomplished according to the models described by Katagiri et al. (1988), Lim et al. (1992), Kim et al. (1997), Casellas et al. (2001), and Tabares and Anglada (2010).

Roughness (Ra, Rt) and flatness deviation of sintered workpieces were measured by a Form Talysurf Intra i60 contact profilemeter with a 2-μm stylus tip radius (r_{tip}), Taylor Hobson μltra and Talymap Gold software. Due to green bodies' fragility and low strength, a non-contact confocal Leica microscope (DCM 3D model) was used to measure surface and roughness parameters, controlled by Leica Scan software and the data analyzed by Talymap Gold software. Input parameters were a 0.25-mm cutoff (λ_c), 0.25-mm single measured length (l_r), 1.25-mm total measured length (l_n), and Gaussian filter to distinguish roughness, waviness, and shape error according to ISO 25,178 and ISO 4287.

Indirect material removal rate (MRR) quantification of the workpieces was used by means of an analytical Shimadzu scale (model AUW-D) after sintering (initial mass, m_i) and U_d-lap grinding (final mass, m_f). MRR was calculated as $(m_i - m_f)$/time.

2.4. U_d-lap grinding

For the dressing operation, brand-new single-point diamond dressers, with a 60° taper and 0.5-mm nose radius geometry (r_p), were used for each test. The dresser was kept perpendicular to the grinding wheel.

For U_d-lap grinding experiments, three different conventional grinding wheels made of different silicon carbide grit sizes (#300, #600, and #800) and hot pressed with an epoxy bond of 350-mm diameter and 25-mm thickness were used.

Filtered water at an 8.33×10^{-5} m^3/s flow rate was applied by flood during dressing. A 1:40 emulsion of semi-synthetic soluble oil (Rocol Ultracut 370) was sprayed using the minimum quantity fluid (MQF) method at 2.78×10^{-7} m^3/s during U_d-lap grinding. The location of the cutting fluid nozzles was the same as that used by Fiocchi (2010, 2014), Fiocchi et al. (2011, 2015), and Fiocchi and Sanchez (2011). A higher cutting fluid flow rate was necessary during dressing to remove the slurry formed on the grinding wheel, thus cleaning it up before U_d-lap grinding.

U_d-lap grinding tests were conducted to analyze the influences of three U_ds and three SiC abrasive sizes on surface finishing of 3Y-TZP specimens (3×3^2 experiments). The main parameters were: U_d = 1, 3, and 5; #300, #600, and #800 SiC; 0.1-mm depth of dressing (a_d); 100-kPa lap grinding pressure (P); and 100-rpm workpiece rotational speed (n_w) and grinding wheel rotational speed (n_g). These final parameters, summarized in Table 1, were defined after a long series of pretests aiming to produce the best surface finishing.

The U_d-lap grinding was interrupted at 5, 10, 15, 20, 25, 30, 40, and 60 min and the workpieces were removed from the holder, cleaned with acetone in an ultra-sound bath, dried, weighed for MRR quantification, and their surface roughness (Ra, Rt) and flatness deviation were measured.

Both dressing and U_d-lap grinding steps were monitored by measuring the main motor electric power (current sensor), applying a Ciber Power Analyzer (CVM NGR 96 model), described in Fiocchi (2010), which is integrated into the machine-tool.

A Nikon and a Carl Zeiss stereo microscope (SMZ 800 and Citoval 2 models, respectively), both linked to a Samtek digital camera (STK 3520 model), as well as PixelView software, were used for grinding wheel optical microscopy.

The clamping technique was brought from the electronic ceramic industry by melting of Thermoplastic Quartz Cement (model 70C from Lakeside) on a glass substrate etched by hydrofluoric acid to enhance adhesion. One workpiece at time was first glued onto the center of the disc using a template to centralize the workpiece on the glass. A QUIMIS hot plate at 100 °C (Q.261.2 model) was used to melt the glue. During cooling of the glue, a second disc and a 2-kg mass were placed over the workpiece in order to homogeneously distribute the molten glue and keep the workpiece's surface parallel to the glass. Next, the smooth face of the disc was put in contact with the vacuum chuck, the vacuum pump turned on, and the vacuum valve closed to hold the disc in position on the chuck. Fig. 3 shows the workpiece fixture sequence.

A 2400-W vacuum cleaner was used to clean up the grinding wheel's surface during dressing and U_d-lap grinding operations in order to avoid any loose particles on the grinding wheel that may have damaged the finishing and/or the workpiece's surface integrity. Therefore, only two-body abrasion is expected. Suction nozzles are strategically located before and after grinding and dressing areas according to Fiocchi (2010, 2014) and Fiocchi et al. (2015), as can be seen in Fig. 4.

3. Results and discussion

3.1. Lap Grinder II

Fig. 4 shows the grinding area of Lap Grinder II and its key elements, such as control panel, servo motor, grinding wheel, vacuum chuck and valve, as well as cutting fluids and suction nozzles.

According to Pahl et al. (2007), the evolution of the machine-tool regarding design methodology is considered an adaptive design, since it kept to known and established solution principles and adapted the embodiment to changed requirements. On the other hand, the original machine-tool based on a modified design that confers on it new features and capabilities is considered a developmental design by Kerala (2002).

The vacuum chuck and glued workpiece showed themselves efficient and practical, with good resistance to cutting fluids and grinding forces in addition to easy cleaning.

The developmental design of the spindle was necessary to clamp the workpiece by a vacuum and to add two degrees-of-freedom to the joint connecting the vacuum chuck and the spindle's shaft. This articulation dynamically compensates for any misalignment, keeping the workpiece's surface always parallel to the grinding

Table 1
Input and output parameters studied through U_d-lap grinding.

Input parameters				Output parameters
Dressing	*U_d-lap grinding*	*Workpiece*	*Grinding wheel*	
a_d = 0.1 mm	P = 100 kPa	3Y-TZP Tosoh	Silicon Carbide (SiC)	Workpiece roughness (Ra, Rt)
60° taper and 0.5 mm dresser nose radius (r_p)	n_g = 100 rpm	1400 °C sintering temperature	Hot pressed epoxy bond	Workpiece flatness deviation (μm)
n_w = 100 rpm	n_w = 100 rpm	29.8 ± 0.15 mm diameter	Ø350 × 25 mm	Dressing and U_d-lap grinding power (W)
8.33×10^{-5} m³/s filtered water	2.78×10^{-7} m³/s 1:40 Rocol Ultracut 370	3.77 ± 0.02 mm thickness	#300	Grinding wheel surface microscopy
Flood	MQF	0.45 μm Ra 7.47 μm Rt	#600	Workpiece 3D profilometry
U_d = 1, 3, and 5	60 min	29.3 ± 1.7 μm flatness	#800	MRR (g/minute)

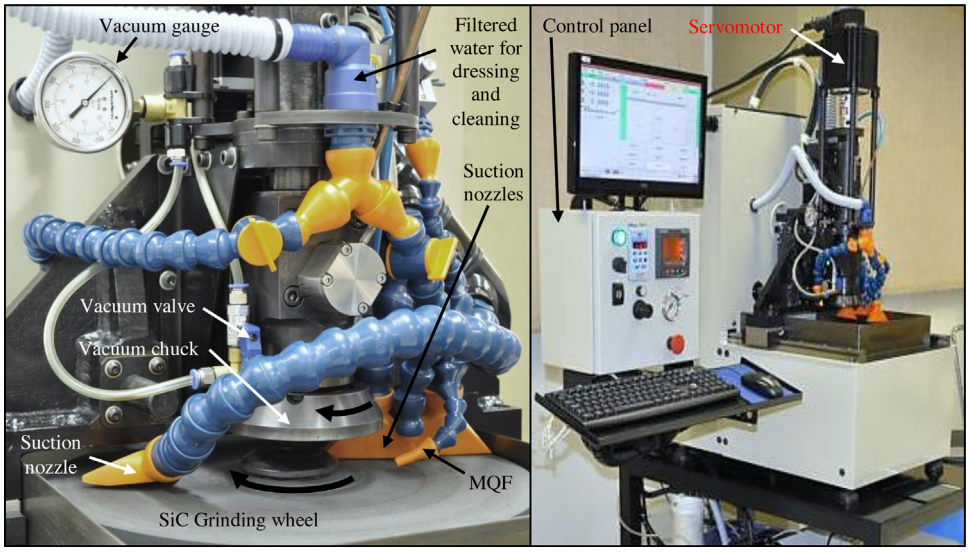

Fig. 4. CNC Fiocchi Lap Grinder II.

wheel. These features resulted in a stiffer and more stable mechanical system. The servomotor offered constant angular velocity to the vacuum chuck, and the new stepping motors and drives prevented the linear axis from resonating. Thus, all the irregularities pointed out were overcome and a robust UP machine-tool design was achieved and validated.

3.2. U_d-lap grinding

3.2.1. Grinding wheel topography

Figs. 5 and 6 show the optical microscopies of 4 × 4 mm areas of the grinding wheels' active/functional surfaces after dressing and 60 min of U_d-lap grinding, respectively. U_d values are arranged in rows and abrasive grit size in columns. Darker regions represent deeper areas of the grinding wheel.

The images showed in Fig. 5 are similar to those found in Fiocchi (2010) and Fiocchi et al. (2011, 2015). The macroeffect was evident for all U_d dressings applied on both #800 and #600 and on the #300 grinding wheel dressed with U_d = 1. After U_d-lap grinding, all grinding wheels (Fig. 6) kept their structures opened without adhesion of material from the workpiece, as opposed to that seen in the machining of AISI 420 stainless steel in Fiocchi (2010) and Fiocchi et al. (2011, 2015). The lower ductility, higher hardness, and lower friction coefficient of the 3Y-TZP as well as the grinding conditions may sustain these findings.

3.2.2. RMS electric power

For those grinding process, i.e., peripheral longitudinal grinding (Fig. 6a), in which the active surface is the cylindrical periphery of the grinding wheel, at a constant distance from its rotational center, the grinding power (P_c) can be calculated as:

$$P_c = F_t \times V_c \quad (1)$$

where F_t is the tangential grinding force and V_c the tangential velocity of the tool (Tönshoff et al., 2002). In such process, for instance, F_t can be accurately obtained by commercial piezo-dynamometers and, hence, P_c can be calculated.

On the other hand, the abrasive process studied does not have a constant relative tangential velocity due to the relative kinematics of the workpiece and grinding wheel (Fig. 6b). Thus, every single point (i) of the tool/workpiece interface has its own $V_{c,i}$. In this particular face grinding with constant pressure and lapping kinematics process, the use of a hall effect sensor is recommended to determine P_c, considering that a dynamometer would not be able to determine local tangential grinding force ($F_{t,i}$).

Commercial piezo-dynamometers provide the most accurate measurement of cutting forces. These transducers have high stiffness, but since they use piezoelectric ceramics, the measurement of static forces over a long period of time may result in significant drift (Byrne et al., 1995), and because of their difficulties for installation in the force loop, the application of piezo-dynameters is restricted (Jemielniak, 1999). Force transducers are also subjected to dynamic influences from the machine/tool/workpiece system (Oliveira and Valente, 2004).

According to Oliveira and Valente (2004), current sensors for power measurement are the simplest and lowest-cost alternative for process monitoring; in addition, their installation is simple, with

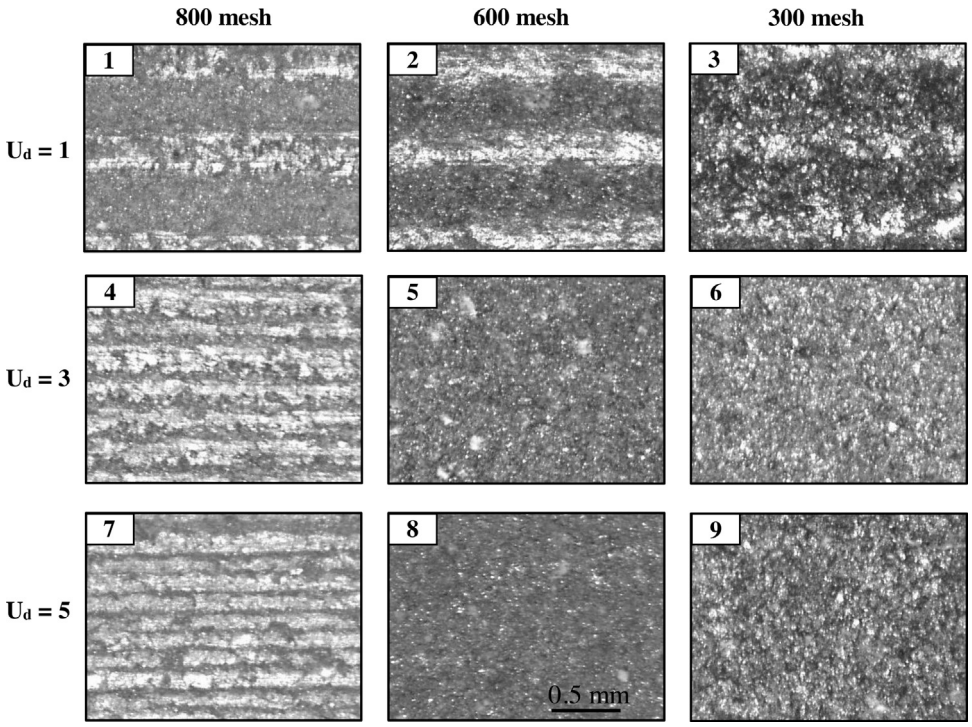

Fig. 5. Optical microscopy of the grinding wheel's active surfaces after dressing. (a_d = 0.1 mm, 0.5-mm nose radius, n_g = 100 rpm, and filtered water applied by flood).

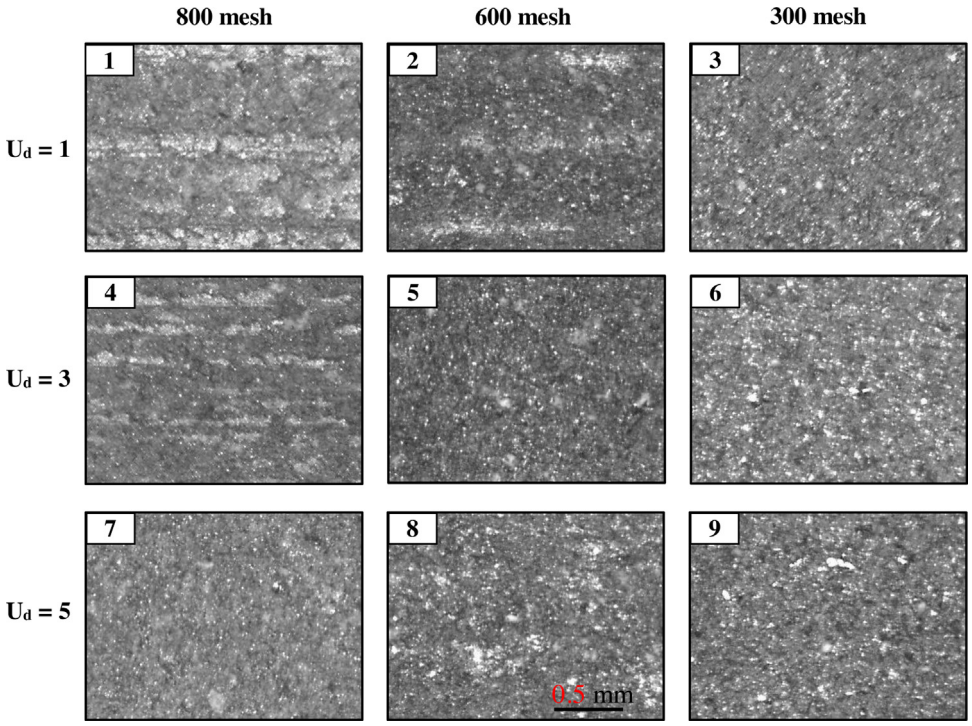

Fig. 6. Optical microscopy of the worn grinding wheel's active surfaces after 60 min of U_d-lap grinding. (P = 100 kPa, $n_g = n_w$ = 100 rpm, and emulsion applied by MQF).

no influence on the system stiffness. The power is usually obtained by measurement of the voltage and electric current at the grinding wheel spindle motor (Malkin and Koren, 1980). Byrne et al. (1995), Jemielniak (1999), and Oliveira and Valente (2004) contend that this method (hall effect/current sensor) is precise and it has low intrusiveness, but it is damped due to the system inertia, i.e., grinding wheel, and the signal processing characteristics needed. This leads to a delayed response that is not important for this research, since the work is not focused on short events. Thus only the relative magnitude of U_d-lap grinding power among the grinding conditions is important in order to reveal the influence of U_d and grinding wheel grit sizes along 60 min of U_d-lap grinding.

3.2.3. Dressing power

The updated machine-tool permits deactivation of the workpiece-holder rotation during dressing. In the older ver-

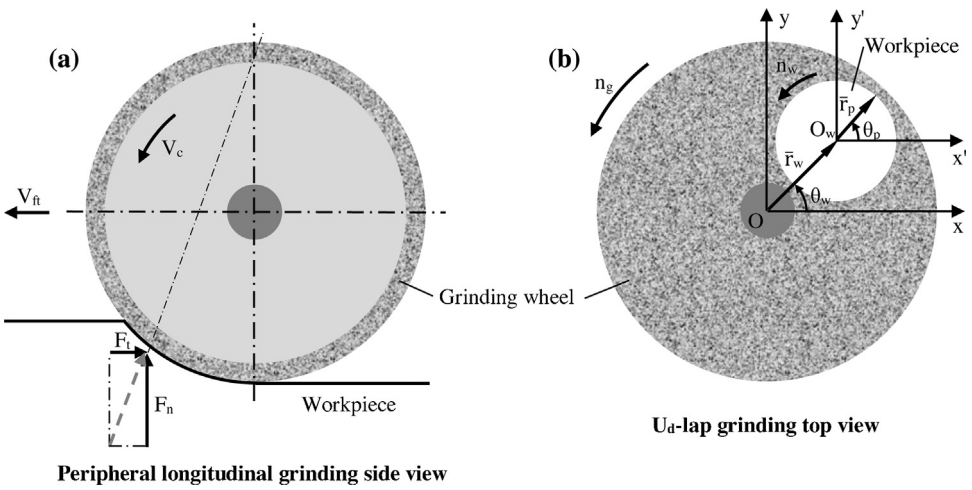

Fig. 7. (a) Discretization of force components in peripheral longitudinal grinding (Tönshoff et al., 2002). (b) Geometrical model for U_d-lap grinding.

sion this was not possible due to the permanent mechanical connection between the workpiece-holder and the main shaft through the flexible shaft (Fiocchi, 2010; Fiocchi et al., 2011). In such case, Lap Grinder II demands less energy by stopping the servomotor and, consequently, the vacuum chuck spindle, during dressing.

As for the reduction in the amount of energy required for dressing, some correlation was expected between the present and earlier results (Fiocchi et al., 2015) regarding dressing power (Fig. 8). Although the current research has used precisely the same grinding wheels, the same dresser's geometry, and exactly the same dressing parameters applied by Fiocchi et al. (2015), there was a change in the RMS dressing's electric power. The #600 and #800 grinding wheels integrities may have been damaged by the age of the tools purchased in 2004. A softening of these grinding wheels, by loosening abrasives particles more easily, was noticed; this caused their macro geometries to deteriorate more rapidly, especially for the #800 grinding wheel.

3.2.4. U_d-lap grinding power

Fig. 9 indicates that, on average, the higher the U_d value, the lower the RMS U_d-lap grinding power: 176.71 W for $U_d = 1$, 173.91 W for $U_d = 3$, and 172.34 W for $U_d = 5$. This graphic suggests, therefore, that, on average, higher U_ds have a tendency to demand less power in zirconia U_d-lap grinding using SiC grinding wheels.

The difference between theoretical and real macro and micro effects over the grinding wheel and the weakening of the epoxy bond can explain those variances. Fig. 10 illustrates some important aspects changed in grinding wheel topography by a single-point diamond dressing, such as the number of active abrasives (cutting edges interacting with the workpiece), as well as the wedge angle (β), rake angle (γ), relief angle (α), and macro porosity.

Such analysis is by no means a trivial task. It depends on abrasive size and friability as well as the "health" of the bond holding these abrasive particles and agglomerates in place, which in a real dressing situation involve diverse macro and micro effects, besides structural damage in grinding wheel, which can be extremely hard to predict, quantify, and qualify. The predominance of one or more effects can thus justify the dispersal of U_d-lap grinding powers depicted in Fig. 9.

3.2.5. Material removal rate

A very important consequence of applying different U_ds is shown in Fig. 11, which presents different conditions of material removal as a function of all U_d-lap grinding situations. The range of the results using the same grinding wheel reinforces the capability of the U_d dressing to modify grinding wheels' aggressiveness. The lowest MRR was 1×10^{-6} g/minute for $U_d = 1$ and #800. The highest, 19 times bigger, happened with $U_d = 5$ and #300.

3.3. 3Y-TZP characterization

Unfortunately, it was not possible to study/focus on exactly the same regions due to lack of a common reference system among the confocal microscopy, contact profilometer, SEM-FEG, XRD, and Raman spectrometer. All analysis happened in the same vicinity, which also represents the characteristics of the entire surface.

3.3.1. 3Y-TZP preparation

Two different magnifications of SEM-FEG of TZ-3Y-E powder are shown in Fig. 12a and b. The raw material presented the predominance of a rounded agglomerate of 0.06 ± 0.03-mm (Fig. 12a) and particle size of 0.08 ± 0.02-μm average diameter (Fig. 12b). Some agglomerate shapes were obtained after drying (Fig. 12c) and granulation/selection (Fig. 12d). Fig. 12e presents the compacted ceramic at 200 MPa, representing the new bigger agglomerates and the residual interagglomerate porosity as described by German (1987). Fig. 12f demonstrates zirconia's 0.35 ± 0.07-μm average grain size achieved by 2 h of sintering at 1400 °C. Table 2 displays the final zirconia's properties.

3.3.2. Profilometry

Uniaxial pressing inducted density gradients in the green bodies, compacted as well explained in literature. Those gradients generated plastic deformations and, therefore, form error in the thin ceramic discs. After the isostatic pressing step those density gradients were considerably reduced, but the form error remained and produced concave and convex opposite surfaces in the same workpiece. The form error increased or decreased depending on the side of the workpiece exposed to the higher temperature inside the furnace during sintering. An amplification of form error was noticed when the concave surfaces were exposed to higher temperatures. On the other hand, better form correction happened when convex surfaces were subjected to higher temperatures. Also observed was an important influence of gravity acceleration during sintering as consequence of deformation of thin ceramic discs that had rested on irregular surfaces.

In the universe of producing near net shapes in UP ceramic manufacturing, the following should be considered: the type of pressing and its associations; the adoption of green ceramic machining to

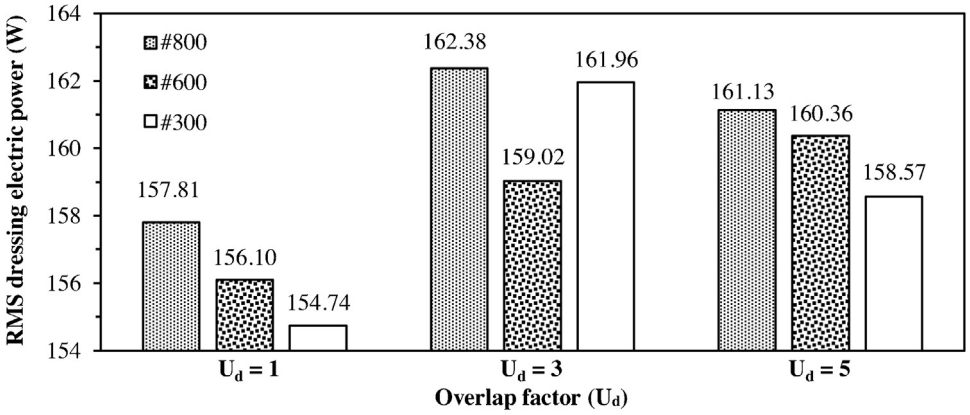

Fig. 8. RMS dressing electric power as function of overlap factor and SiC grit size. (a_d = 0.1 mm, 0.5-mm nose radius, n_g = 100 rpm, and filtered water applied by flood).

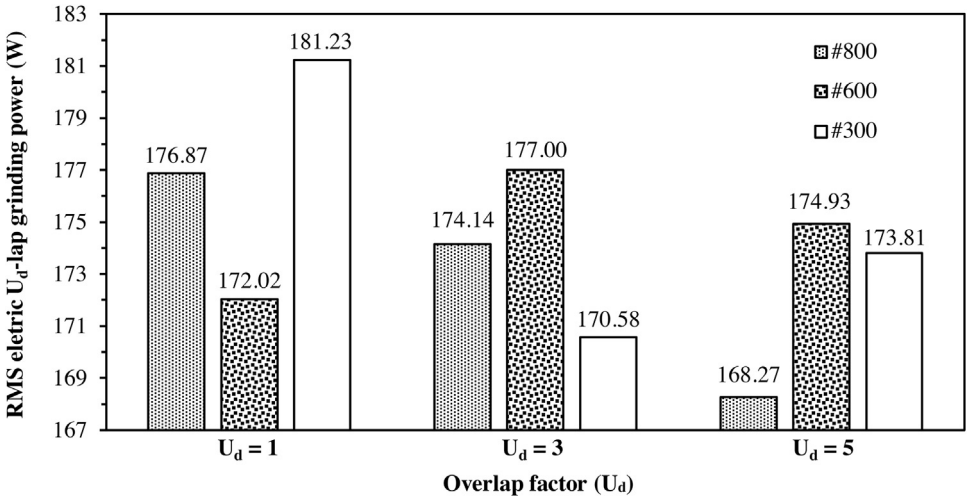

Fig. 9. RMS U_d-lap grinding electric power as function of overlap factor and SiC grit size. (P = 100 kPa, $n_g = n_w$ = 100 rpm, and emulsion applied by MQF).

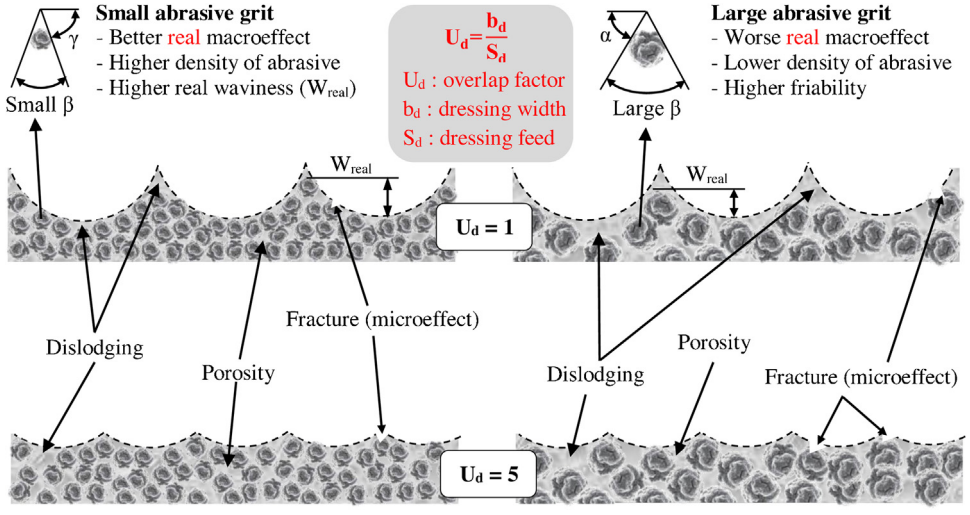

Fig. 10. Schematic representation of the real and theoretical macro geometry (dashed lines) of the grinding wheels depending on the abrasive size and overlap factor (U_d).

Table 2
Final zirconia discs properties after sintering.

TZ-3Y-E			
Micro hardness (HV)	*Opened porosity (%)*	*Density (g/cm³)*	*Average grain size (μm)*
1414.10 ± 339.28	0.002 ± 0.001	6.0 ± 0.06	0.35 ± 0.07

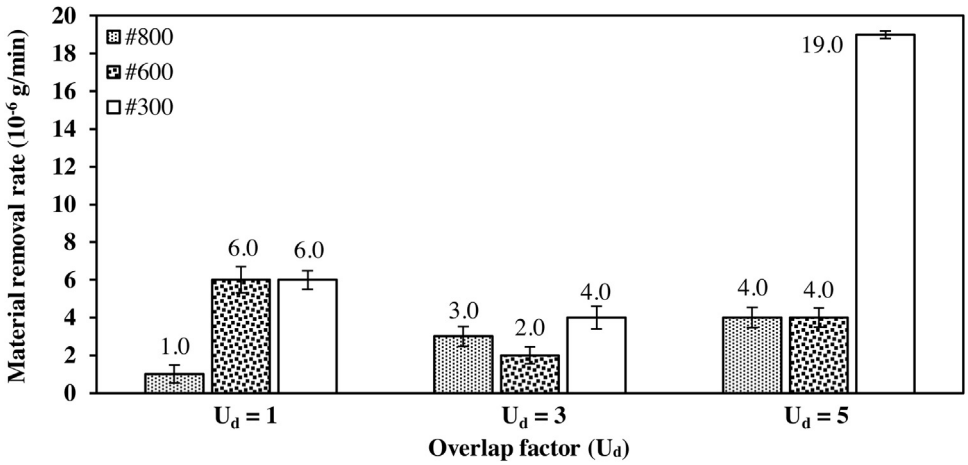

Fig. 11. MRR (g/minute) as function of overlap factor and SiC grit size. (P = 100 kPa, $n_g = n_w$ = 100 rpm, and emulsion applied by MQF).

shape the part and also remove the highest-density gradients in outside layers; the flatness of the base, and the temperature distribution inside the furnace. All these consideration will minimize the effects of heterogeneous pressing and sintering shrinkage. The judicious choice of these parameters, therefore, shall result in less machining time for correction of form, which will focus mainly on finishing.

3.3.3. Surface roughness

For all tested conditions, there was a sharp diminishing in the values of surface roughness in the first 5 min and a slight variation of surface quality until the end of 60 min of U_d-lap grinding. As can be seen in Fig. 13, all three graphics had the same scaling.

For the #800 dressed with U_d = 1 and 3, the roughness decreasing rate is practically the same and several times higher than for U_d = 5 in the first 5 min. The worst performance can be explained by the premature wear of the #800 grinding wheel dressed with U_d = 5, which lost its macro effect sooner, as can be noticed comparing Figs. 5-7 and 6-7.

The #600 grinding wheel did not show a visible macro effect for U_d = 3 and 5 (Fig. 5-5 and 5-8). However, the micro effect may have positively influenced surface roughness by offering new cutting edges with different angles and lower depth of cut as well as sufficient grinding wheel porosity to carry debris and cutting fluid, therefore showing that the U_d through a single-point diamond dressing changes grinding wheel aggressiveness. Fig. 6-5 and 6-8 show similar topographies and may explain the similarity in roughness produced by the #600 dressed with U_d = 1 and 5 during the last 20 min.

The influence of U_d was more evident over the #300 grinding wheel. During the first 5 min all U_ds produced quite similar roughness decreasing rates. The best roughness came from U_d = 5 and the worst one from U_d = 3.

Figs. 14 and 15 present Ra (nm) and Rt (μm) roughness parameters values at the end of 60 min of U_d-lap grinding, respectively.

The idea behind Fig. 10 can justify the roughness depreciation with the substantial increase of deeper risks produced by the #600 and #800 grinding wheels; higher Rt values are shown in Fig. 15.

TZ-3Y-E is harder than the AISI 420 stain steel studied by Fiocchi et al. (2015) and thus no material is impregnated into the grinding wheel's surface, resulting in higher abrasive protrusion that may depreciate finishing, but keeps the tool cleaner and with opened porosity. On the other hand, the constant abrasive exposure associated with the higher hardness of zirconia wears the grinding wheel easily.

3.3.4. Topography

Fig. 16 and 17 illustrate confocal microscopy of a green and a fired piece, respectively. Surface finishing improved 36% in arithmetic mean height (Sa) from green (0.71 μm) to the sintered (0.52 μm) stage, as well as producing flatter and smoother areas.

Fig. 18 represents workpieces' surface obtained by confocal microscopy after 60 min of U_d-lap grinding. In this figure can be seen a predominance of ductile cutting, absence of cracks, and pattern of aleatoric scratches. At least two levels of scratching can be visualized: one severe with larger width and depth, and another gentler with shallow marks. In both cases the microcutting seems to be the major ductile removal mechanism in all conditions studied.

In some workpieces there are still remnants of areas from the sintered genitor surface, such as the presence of opened pores, depressions with spherical geometry, and non-machined areas. In the context of this work, those zones are classified as irregularities and might be removed by increasing the U_d-lap grinding time, since the studied cutting conditions provided low MRR.

The condition of U_d = 1 and the #300 grinding wheel raised a suspicion that besides ductile cutting, there was also microplowing and plastic displacement of material, as demonstrated in Fig. 19.

The white arrows point to microcutting marks. The white dashed circles delimit areas of plastic deformation at the intersection of the scratches, which reveals the chronological sequence of events. The newest scratches have overshadowed the predecessor ones.

The black arrows point out possible microcracks. However, SEM proved that those regions came from plastic dislocation of material toward the center of the scratch. Another fact that supports this thesis is that the white left arrow points to a deeper scratch without cracking. How could a less aggressive condition, pointed out by the black arrows, generate such failure?

The presence of plastic deformation put forward the idea that strain hardening may be taking place. In such case, by the time its limit is reached, the material suffers brittle fracture. This discussion will be resumed by SEM analysis.

3.3.5. Flatness deviation

Fig. 20 displays a wide variety of flatness deviation and reinforces the ability that the single-point diamond dressing has to modify grinding wheels' characteristics in U_d-lap grinding.

3.3.6. SEM-FEG

The quality of the images acquired by the SEM-FEG is much better than those obtained by confocal microscopy; however, the SEM employed was not capable of measuring roughness. Figs. 18 and 21

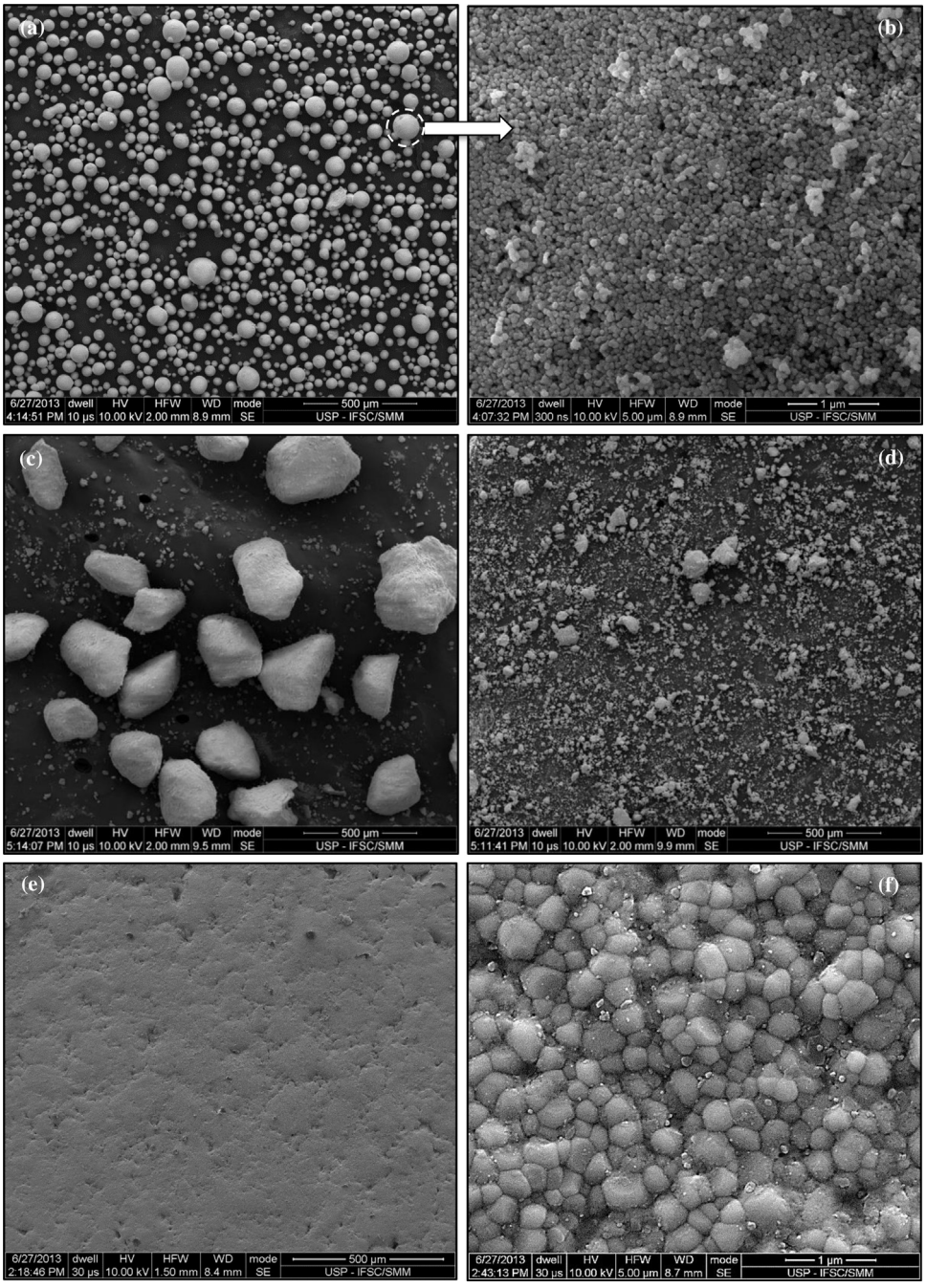

Fig. 12. SEM-FEG of Tosoh TZ-3Y-E: (a and b) raw material; (c) dried and (d) granulated/selected by #80 (180 μm) sieve; (e) isostatically pressed at 200 MPa; (f) sintered by 2 h at 1400 °C and a heating/cooling rate of 3.89 °C/minute.

represent the same surfaces shown by different techniques. Such comparison is important to display the differences in interpretation of the surfaces depending on the microscopy technique used.

The confocal and electron microscopy images demonstrate removal mechanisms such as ***microcutting***, ***microplowing***, and ***microgrooving***. During both microscopy procedures the workpieces had all of their surfaces scanned, and no crack introduced by U_d-lap grinding was detected.

The microcutting was more active at the beginning of the process, when the abrasives were still sharp. The other mechanisms happened practically during the entire machining time, becoming more evident with the wear of the cutting edges that increased the tip's radius, exactly as described by Marsh (1964).

Fig. 22a shows the microplowing, which plastically dislocates material to the border of the furrow. The microgrooving can be seen in Fig. 22b; zirconia's grains are smashed, minimizing the grain boundaries by means of longitudinal plastic deformation of the ceramic material.

In some circumstances the abrasive penetration into the workpiece provided a cutting cross section that promoted ductile cutting with low residual plastic deformation. This specific cutting conditions did not raise material at the border of the scratch and left parallel abrasive marks in the cutting direction at the bottom of the scratch. Fig. 22c illustrates this microcutting mechanism.

According to Schinker and Döll (1987), microplowing and microgrooving mechanisms promote not only lateral deformation, but also the compression of the material in the direction of

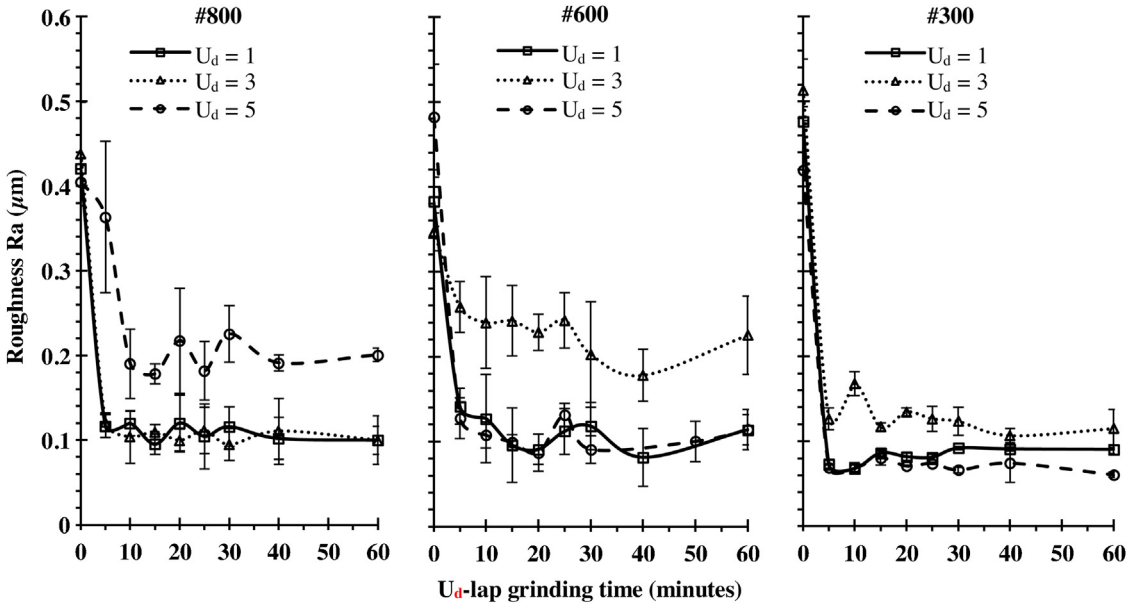

Fig. 13. Roughness (Ra) versus time for different SiC sizes and U_ds. (P = 100 kPa, $n_g = n_w$ = 100 rpm, and emulsion applied by MQF).

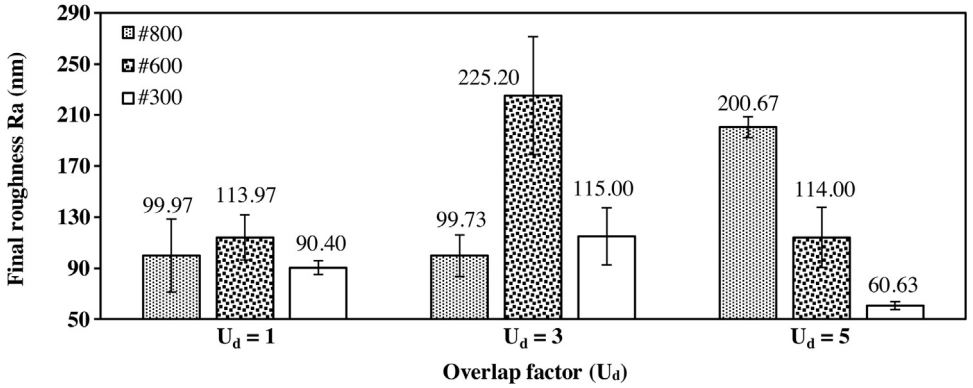

Fig. 14. Final roughness (Ra) after 10 min of U_d-lap grinding for different SiC grit sizes and U_ds. (P = 100 kPa, $n_g = n_w$ = 100 rpm, and emulsion applied by MQF).

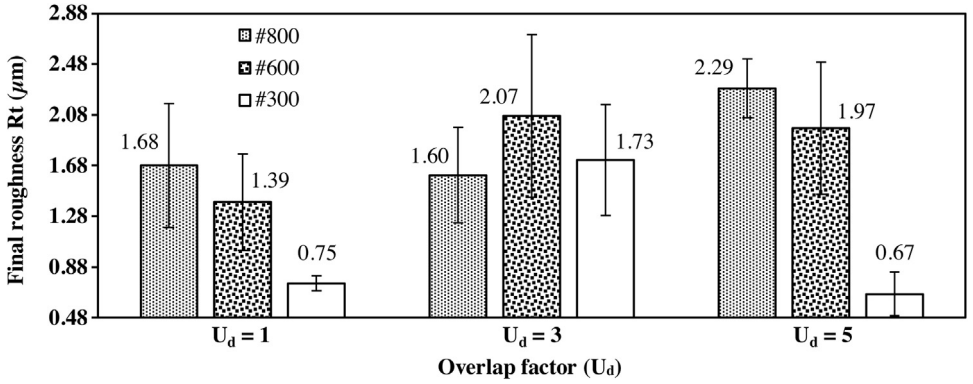

Fig. 15. Final roughness (Rt) after 10 min of U_d-lap grinding for different SiC grit sizes and U_ds. (P = 100 kPa, $n_g = n_w$ = 100 rpm, and emulsion applied by MQF).

machining. By increasing depth of cut the microcutting becomes predominant again. This was one of the explanations found to justify the best roughness produced by the largest abrasive grit (#300 SiC), which also has higher friability.

The SEM images show that U_d-lap grinding has achieved plasticity conditions of 3Y-TZP, which lead us away to believe that the nanometric surface finishing was produced mainly by ductile microcutting and pulverization removal mechanisms. In the first mechanism, the volume of removed material is equal to the scratch volume left. It is believed that the second mechanism happens due to successive plastic deformation accumulated by 3Y-TZP in distinct directions (defects) that has achieved a critical strain state, in which microcracks were not only nucleated, but also formed a recrystallized layer of nanometric thickness according to Tabares

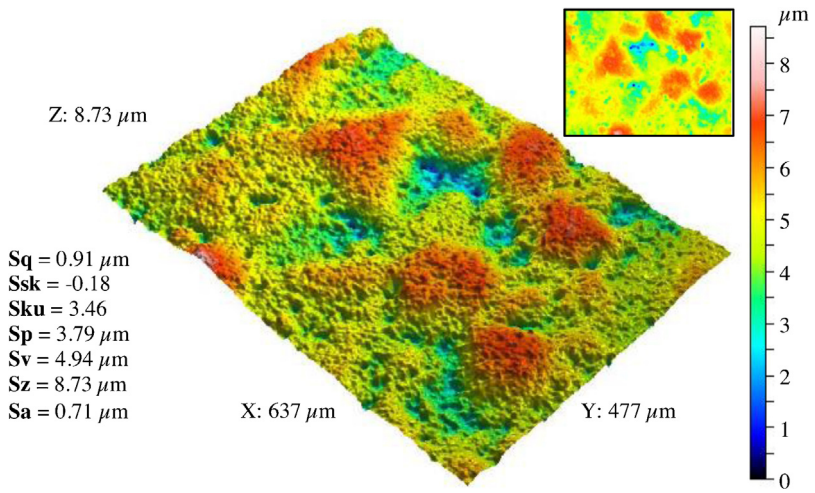

Fig. 16. Confocal microscopy (Leica DCM 3D) of a green piece. 20× objective, dark field, and monochromatic light.

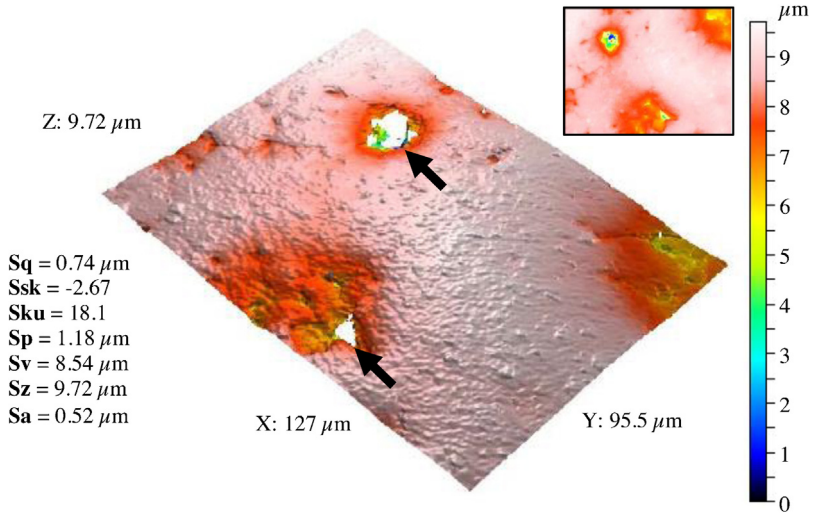

Fig. 17. Confocal microscopy (Leica DCM 3D) of a sintered piece. 100× objective, bright field, and white light.

et al. (2011). This specific removal condition can be associated with metal hardening as a consequence of cold working (strain hardening), which produces very small fragments of material (debris), as well illustrated in Fig. 22d. It is also believed that the last removal mechanism is a consequence of low-cycle fatigue, producing a smooth and practically not scratched surface, as shown in some areas of Fig. 22c.

3.3.7. Raman spectroscopy

Fig. 23 presents Raman spectra of the workpieces submitted to the nine U_d-lap grinding conditions. This figure also contains the spectra of a workpiece as sintered as well as a compacted monoclinic phase zirconia. Vertical black and red lines are superimposed on the graphic in order to help differentiate tetragonal (t) and monoclinic (m) Raman intensities.

The volume percentage of the monoclinic phase was lower than 1%, according to Table 3, which presents different approaches for determining the martensitic transformation. The results were quite similar in each applied theory. Considering those values, the monoclinic phase may be negligible.

3.3.8. XRD

Fig. 24 presents x-ray diffraction patterns for (1) raw material (Tosoh TZ-3Y-E) as supplied, (2) sintered 3Y-TZP, (3) sintered 3Y-TZP after 60 min of U_d-lap grinding using #300 SiC dressed with $U_d = 5$, $P = 100$ kPa, $n_g = n_w = 100$ rpm, and 1:40 emulsion applied by MQF, and (4) compacted monoclinic powder without binder pressed at 80 MPa.

The raw material has traces of the monoclinic phase, as indicated by the purple arrows in the vicinity of $2\theta = 33^\circ$ and 36.5° (Fig. 24-1). Sintering resulted in a fully tetragonal material (Fig. 24-2).

Fig. 24 shows the XRD patterns for all nine U_d-lap grinding conditions studied.

The #600 and #800 grinding wheels practically did not alter the spectra in relation to the sintered workpiece, only tenuous, asymmetric, left broadening around 35°. The singularity was more pronounced using the #600 grinding wheel.

Two characteristic phenomena arising from U_d-lap grinding using the largest abrasive grit were observed. These were the asymmetric broadening of tetragonal peaks near 35° and 59° (black arrows), and reversal of the intensity of the tetragonal peaks at 40° and 41° (Figs. 24-3 and 25). Virkar and Matsumoto (1986), Mehta et al. (1990), and Tabares et al. (2011) affirm that reversal occurs due to ferroelastic domain switching, which can be explained as a reorientation of the crystallographic planes at the level of crystallite. The asymmetric broadening may also indicate a superficial grain refinement. This finding is in agreement with Tabares et al. (2011) that

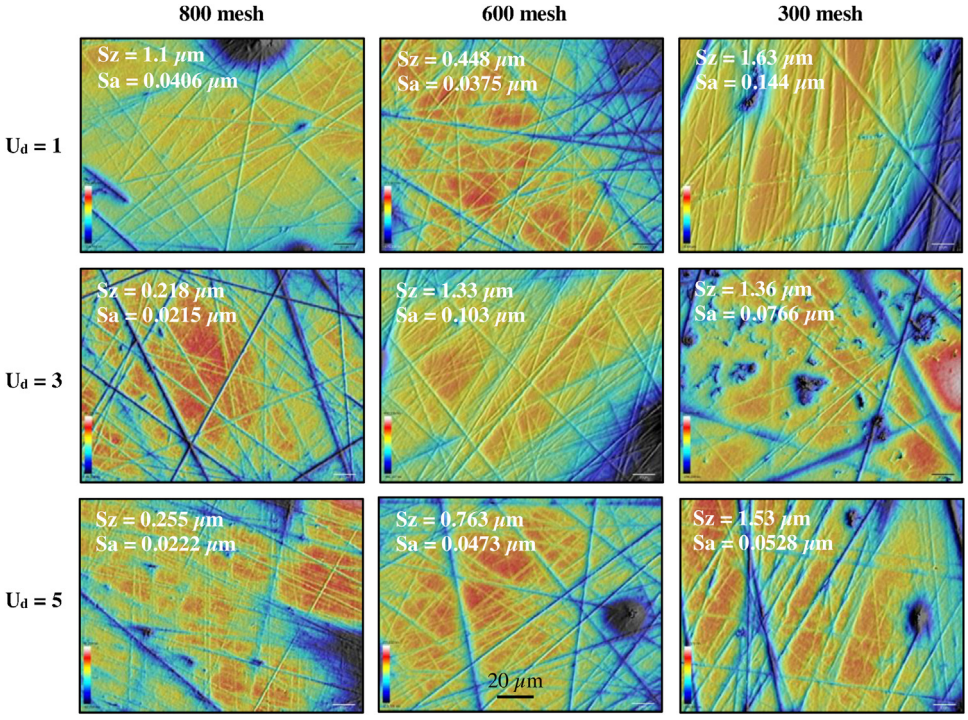

Fig. 18. Confocal microscopy (Leica DCM 3D) after 60 min of U_d-lap grinding with 9 different conditions. 100× objective, bright field, and white light.

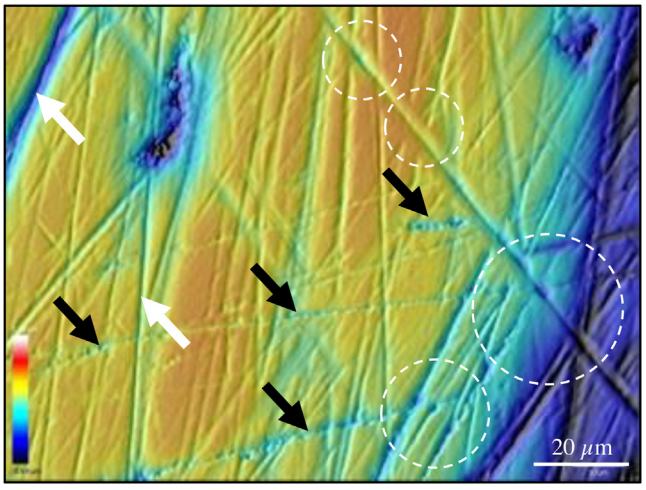

Fig. 19. Confocal microscopy (Leica DCM 3D) of a surface produced by a #300 SiC grinding wheel dressed with U_d = 1. 100x objective, bright field, and white light.

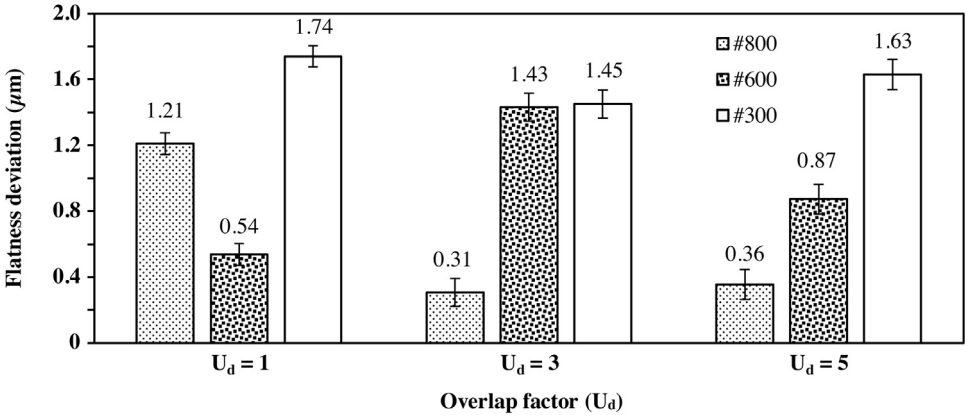

Fig. 20. Flatness deviation after 60 min of U_d-lap grinding, as a function of the overlap factor for different SiC grit sizes (P = 100 kPa, $n_g = n_w$ = 100 rpm, and emulsion applied by MQF).

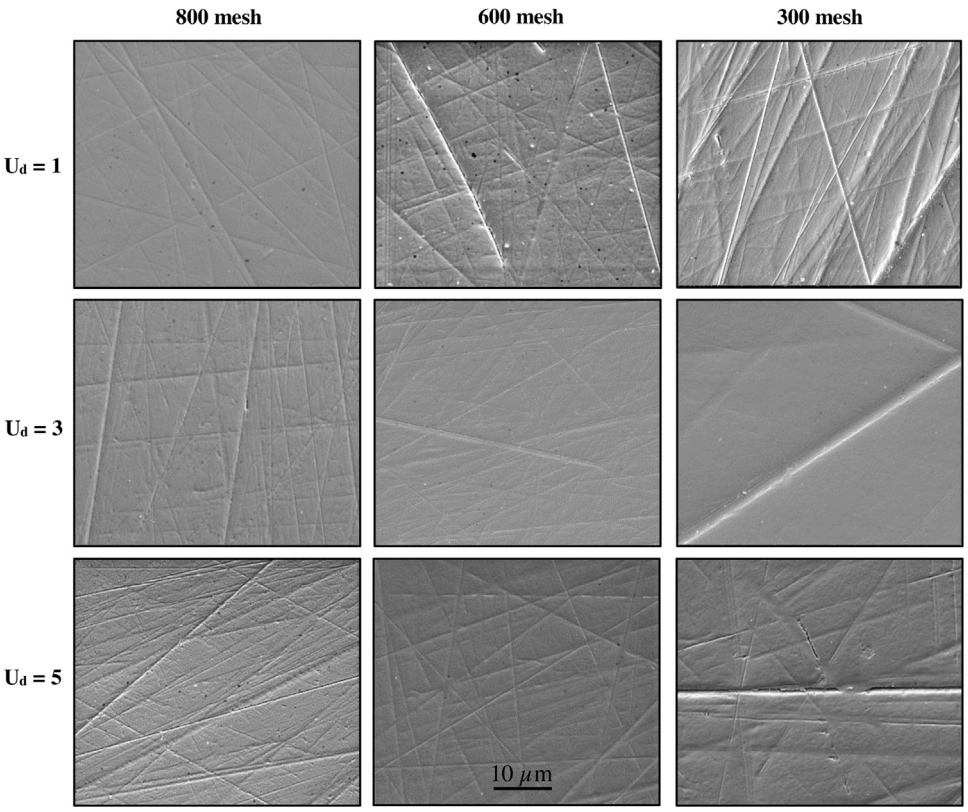

Fig. 21. SEM-FEG after 60 min of U_d-lap grinding with 9 different conditions.

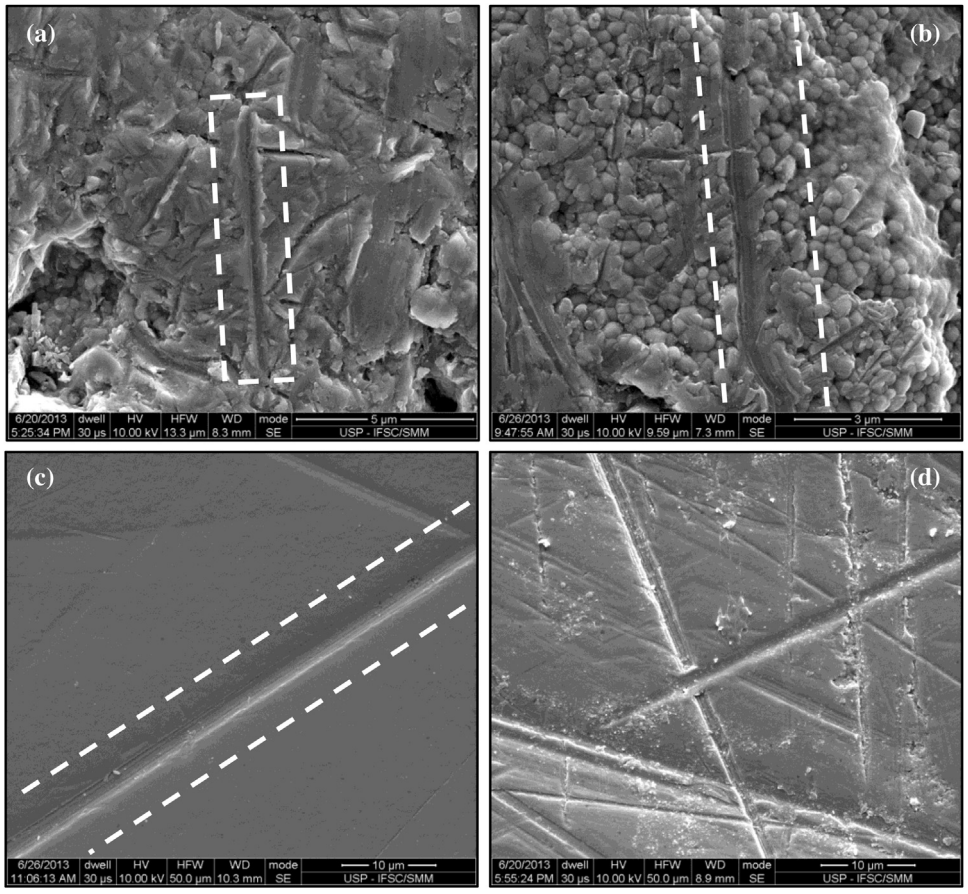

Fig. 22. SEM-FEG of (a) microplowing, (b) microgrooving, (c) microcutting/scratching, and (d) chips produced by U_d-lap grinding.

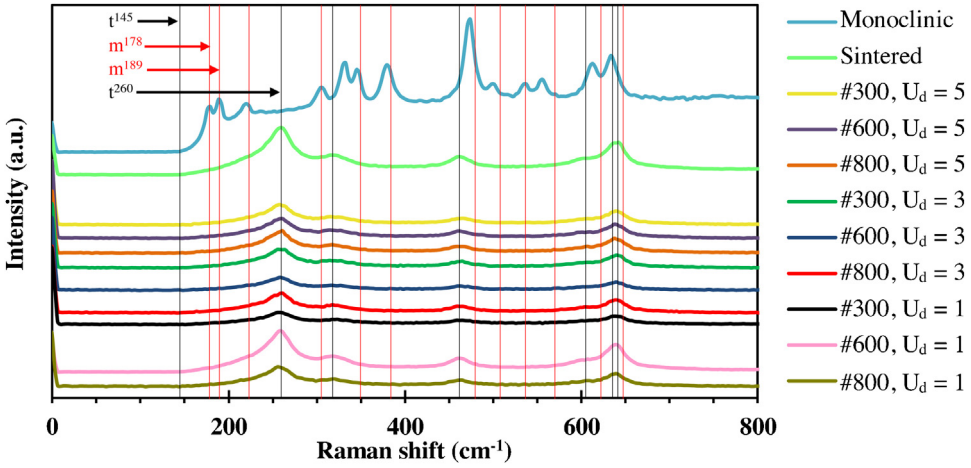

Fig. 23. Raman intensity versus Raman shift (cm^{-1}) of the nine U_d-lap grinding conditions applied in 3Y-TZP, 3Y-TZP as sintered, and a compacted monoclinic phase zirconia. Vertical black and red lines added to the graphic to indicate Raman shift of tetragonal and monoclinic phases, respectively, according to Pezzotti and Porporati (2004).

Table 3
Volume percentage of monoclinic phase (V_m) measured by Raman spectroscopy in U_d-lap ground workpieces.

Author/equation	Parameter		Grinding wheel mesh	Overlap factor (U_d)	V_m (%)	V_m max. [%]	V_m min. [%]
	k	δ					
Clarke and Adar (1982)	0.97	1	800	1	0.50		
			600	1	0.47		
			300	1	0.50		
			800	3	0.50		
			600	3	0.50	–	–
			300	3	0.50		
			800	5	0.50		
			600	5	0.50		
			300	5	0.50		
Katagiri et al. (1988)	0	2.2 ± 0.2	800	1	0.48	0.50	0.46
			600	1	0.49	0.51	0.47
			300	1	0.48	0.50	0.46
			800	3	0.48	0.50	0.46
			600	3	0.48	0.50	0.46
			300	3	0.48	0.50	0.46
			800	5	0.48	0.50	0.46
			600	5	0.48	0.50	0.46
			300	5	0.48	0.50	0.46
(1992)	1	0.33 ± 0.33	800	1	0.75	1.0	0.60
			600	1	0.73	1.0	0.57
			300	1	0.75	1.0	0.60
			800	3	0.75	1.0	0.60
			600	3	0.75	1.0	0.60
			300	3	0.75	1.0	0.60
			800	5	0.75	1.0	0.59
			600	5	0.75	1.0	0.60
			300	5	0.75	1.0	0.59
(1997)	–	–	800	1	0.20		
			600	1	0.20		
			300	1	0.20		
			800	3	0.20		
			600	3	0.20	–	–
			300	3	0.20		
			800	5	0.20		
			600	5	0.20		
			300	5	0.20		
Casellas et al. (2001)	–	–	800	1	0.53		
			600	1	0.52		
			300	1	0.53		
			800	3	0.53		
			600	3	0.53	–	–
			300	3	0.53		
			800	5	0.53		
			600	5	0.53		
			300	5	0.53		

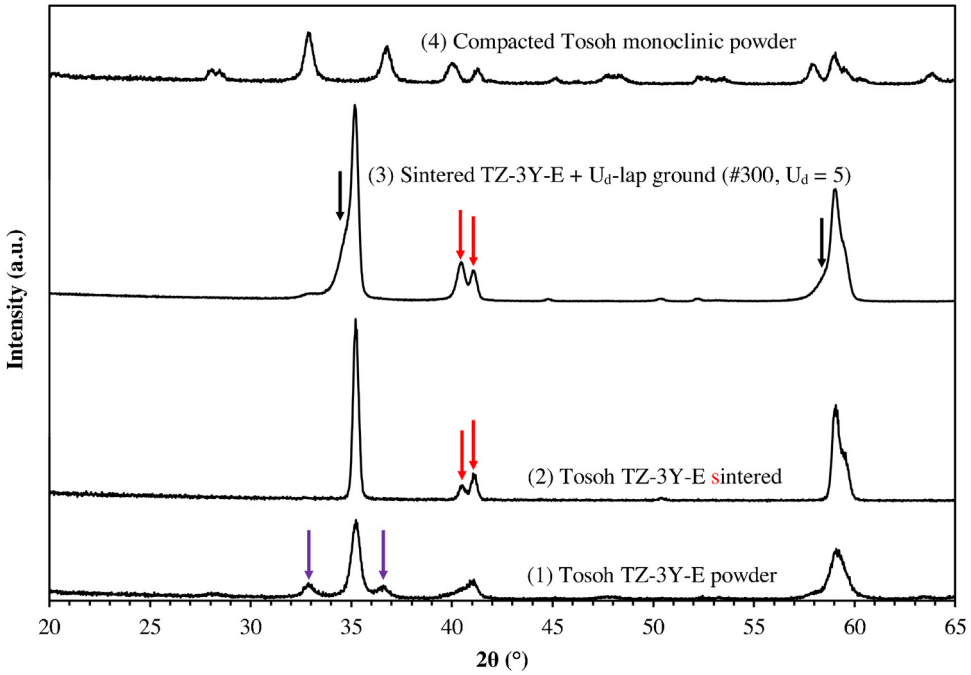

Fig. 24. X-ray diffraction patterns for (1) Tosoh TZ-3Y-E powder as supplied, (2) sintered 3Y-TZP (2 h at 1400 °C), (3) sintered 3Y-TZP after 60 min of U_d-lap grinding using #300 SiC dressed with $U_d = 5$, $P = 100$ kPa, $n_g = n_w = 100$ rpm, and 1:40 emulsion applied by MQF, and (4) compacted monoclinic powder without binder pressed at 80 MPa.

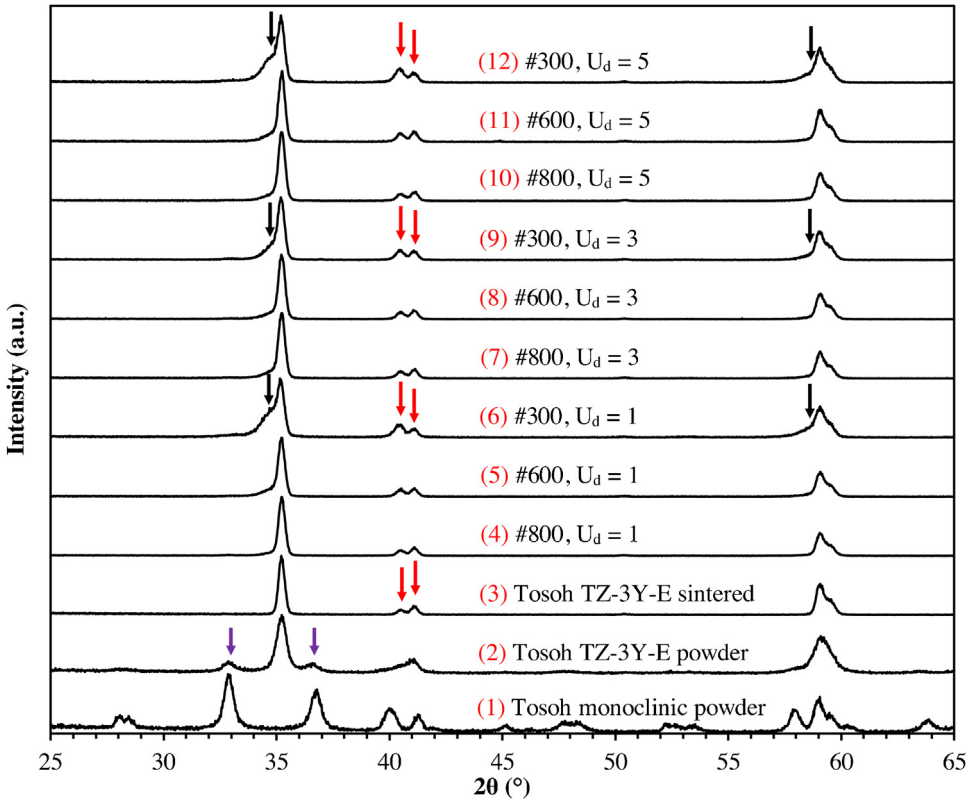

Fig. 25. X-ray diffraction patterns for (1) compacted monoclinic powder, (2) Tosoh TZ-3Y-E powder as supplied, (3) sintered 3Y-TZP, (4-12) sintered 3Y-TZP after 60 min of U_d-lap grinding using $P = 100$ kPa, $n_g = n_w = 100$ rpm, and 1:40 emulsion applied by MQF.

found a recrystallized zone of grains of ~20 nm diameter in ground 3Y-TZP.

Tabares et al. (2011) also showed that the asymmetry observed in the spectrum of ground zirconia is related to the overlapping of the tetragonal and rhombohedral phases. The rhombohedral phase has been associated with distortion of the cubic phase in the [1 1 1] direction according to many authors, such as Hasegawa (1983), Kitano et al. (1988), Mitra et al. (1993), and Tabares et al. (2011). Therefore, the probability of finding a rhombohedral grain is equal to the probability of finding a cubic grain. On the other hand,

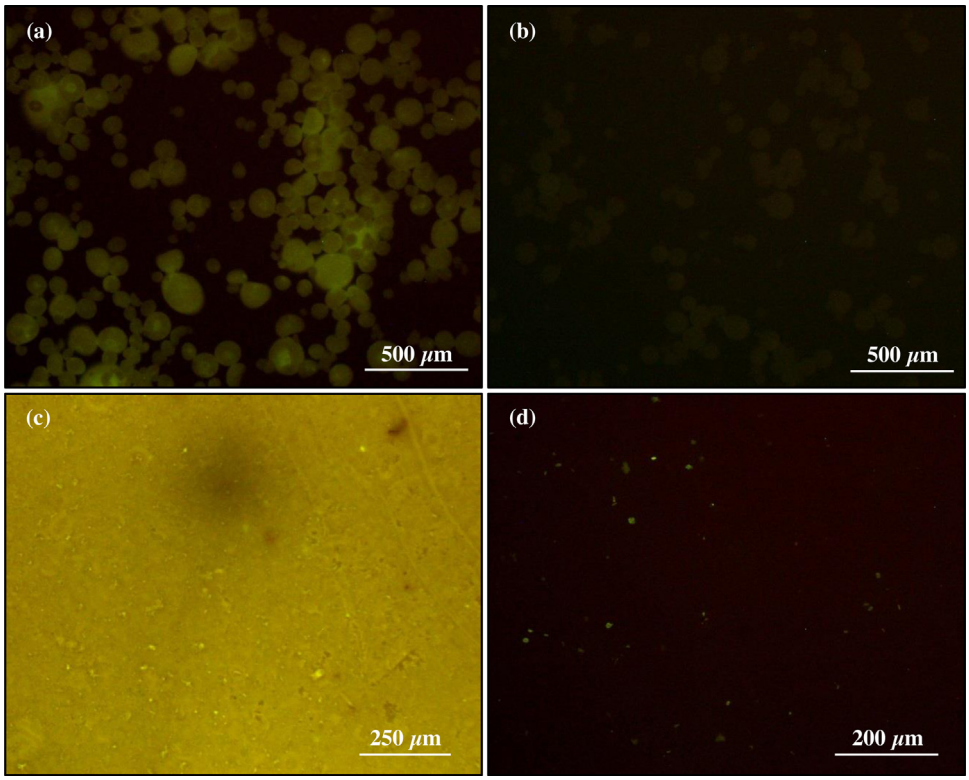

Fig. 26. Optical fluorescence microscopy of (a) Tosoh zirconia monoclinic powder, (b) Tosoh TZ-3Y-E powder, (c) compacted body of Tosoh zirconia monoclinic powder pressed at 80 MPa, and (d) sintered TZ-3Y-E workpiece subjected to 60 min of U_d-lap grinding with the #300 SiC grinding wheel dressed with $U_d = 5$, $P = 100$ kPa, $n_w = n_g = 100$ rpm.

Hasegawa (1983), Burke and Rainforth (1997), and Tabares et al. (2011) argued that the rhombohedral phase is stable only under high compressive stress at ambient temperature.

According to Tabares et al. (2011), from XRD spectra it is clear that peak broadening is a consequence of an overlap of the (1 1 1) tetragonal peak with another symmetrical peak, corresponding to the reflection of the (1 1 1) plane of the cubic phase moved to the left of its position in as sintered. If the cubic phase undergoes the same texture observed on the tetragonal and monoclinic phase, their {1 1 0} plane will be oriented approximately parallel to the surface. This configuration would explain the shift of the (1 1 1) cubic peak to the left side, when a biaxial compressive stress is imposed on the surface plane.

The Raman spectroscopy, that analyzed the surface by a confocal technique, demonstrated practically no t → m phase transformation. XRD is a volumetric technique (cps/volume or mass) and has also indicated that there was no monoclinic phase inside the analyzed volume. Therefore, the association of the two techniques confirmed that the nine U_d-lap grinding conditions studied did not incite martensitic transformation.

The comparison of these results with those found by Tabares et al. (2011) indicates the superiority of the U_d-lap grinding to the peripheral longitudinal grinding. This last grinding process produced three severe microstructural changes, which are clearly divided into three regions from the surface: (1) recrystallized zone with a grain of ~20-nm diameter; (2) plastically deformed zone, and (3) t-m phase transformation zone.

Table 4 represents the quantitative analysis proposed by the Toraya et al. (1984a,b) and Sato et al. (2008) equations.

A maximum volume of 0.1% of monoclinic phase was found in all U_d-lap ground workpieces. Although it is clear that the two techniques cannot be compared without the necessary correction of the analyzed volume and absorbed radiation, both results indicate that the level of transformation in the lap ground material is practically negligible. Hence, the U_d-lap grinding did not form the third region described by Tabares et al. (2011), keeping the desired tetragonal phase, which has superior mechanical properties.

Table 4
Volume percentage of monoclinic phase (V_m) measured by XRD in U_d-lap ground workpieces.

Author/equations	Grinding wheel mesh size	Overlap factor (U_d)	V_m (%)
Toraya et al. (1984a,b) and Sato et al. (2008)	800	1	0.033
	600	1	0.042
	300	1	0.101
	800	3	0.038
	600	3	0.034
	300	3	0.057
	800	5	0.037
	600	5	0.035
	300	5	0.077

Even with the detection of a very low monoclinic phase, it can be noticed that there is a tendency that more aggressive cutting conditions (larger abrasive grit and lower U_d) provoke more phase transformation than gentle ones.

The low percentage of martensitic transformation presented in the outside volume can be consequence of tender tribological conditions achieved by U_d-lap grinding—for instance, shallow depth of cut, low relative velocity (<2 m/s), cutting temperature close to ambient, predominance of ductile removal, and tetragonal phase stabilization reinforced by compressive residual stress.

The #300 grinding wheel offered the best surface roughness but also the highest crystallographic damage on 3Y-TZP, probably due to higher cutting specific pressure that plastically deformed the surface. The lowest Ra roughness should also be a consequence of the higher friability of the #300 SiC abrasive grit.

The correct choices of the U_d-lap grinding cutting conditions must, therefore, take into account not only roughness output, but also crystallographic changes that may influence the life of the part depending on its application. If it is demonstrated that the U_d-lap grinding causes compressive residual stress, the studied abrasive process should occupy a prominent position among the UP grinding processes of ceramic parts susceptible to fatigue and/or LTD.

3.3.9. Optical fluorescence

Fig. 26 shows four optical fluorescence images and reveals that the monoclinic zirconia powder fluoresces under violet light excitation (Fig. 26a). The zirconia doped with yttria (TZ-3Y-E) did not present fluorescence (Fig. 26b). Fig. 26c illustrates the strong fluorescence of a compacted body pressed at 80 MPa without binder. Fig. 26d demonstrates homogeneously distributed fluorescence on a sintered workpiece subjected to 60 min of U_d-lap grinding with the #300 SiC grinding wheel dressed with $U_d = 5$, $P = 100$ kPa, $n_w = n_g = 100$ rpm. The other eight images are not shown because they are qualitatively similar.

Although the literature reports the use of photoluminescence as a tool to study electronic band transitions, structure, defects, chemical composition (Lai et al., 2005), and residual stress (Sheng and Todd, 2011), there has not been seen either an image or a protocol aimed at visual differentiation of the zirconia phases inside the visible electromagnetic spectrum. Considering the XRD and Raman analysis, the fluorescent spots upon U_d-lap ground workpieces cannot be considered a consequence of martensitic transformation, but other defects such as compressive stress that may have stabilized the rhombohedral phase.

4. Conclusions

This paper investigated the U_d-lap grinding process and its machine-tool design aiming at UP manufacturing of advanced ceramics. Influences of three different overlapping factors on dressing (U_d) and three abrasive grit sizes of conventional SiC grinding wheels were analyzed on flat surface finishing of dense 3Y-TZP discs in a ductile regime of material removal. The key findings of this experimental study were:

- The design methodology was successful for supporting to achieve all design requirements in the second version of the CNC Fiocchi Lap Grinder. The efficient machine-tool and U_d-lap grinding process were capable of manufacturing flat 3Y-TZP surfaces with nanometric finishing without introducing critical defects.
- Differences between theoretical and real macro and micro effects over the grinding wheels after single-point diamond dressing, epoxy bond strength, abrasive protrusion, abrasive grit size and abrasive friability play a key role in U_d-lap grinding.
- The consequences of applying different U_ds are the distinct outputs regarding roughness, MRR, and flatness deviation; the range of these results, using the same grinding wheel, reinforces the capability of the U_d dressing to modify grinding wheels' aggressiveness and surface finishing.
- Nanometric surface finishing was produced mainly by microcutting and pulverization removal mechanisms.
- The best finishing, Ra = 60.63 nm, came from the #300 grinding wheel dressed with $U_d = 5$. Flatness deviation of 0.308 μm was obtained through the #800 grinding wheel and $U_d = 3$.
- Raman spectroscopy and XRD indicated that the level of martensitic transformation in the U_d-lap ground material was negligible. The occurrence and magnitude of phase change induced by removal conditions can be used as a scientific tool for evaluating the quality of UP material removal processes.
- Monoclinic zirconia powder fluoresced under violet light excitation.
- In UP manufacturing of advanced materials, all production steps must be controlled. Considering that fired advanced ceramics are materials that are hard, difficult and expensive to machine, an optimized manufacturing route should consider a near-net-shape production, in which material removal processes should be applied mainly for improving surface finishing.
- U_d-lap grinding-generated a pattern of isotropic nanometric finishing due to cycloidal trajectories regardless of the surface orientation and form error of the workpiece, was strongly influenced by grinding wheel's flatness.
- There is no report of an abrasive process capable of achieving similar nanometric finishing with the same micrometric grit size and type of abrasive. The U_d-lap grinding can replace the engagement of processes such as grinding, lapping, and polishing of advanced ceramics.

Acknowledgments

The authors would like to thank Fundação de Amparo à Pesquisa do Estado de São Paulo (FAPESP), Brazil, for financial support (Grants 2002/06452-6, 2008/50233-3, and 2011/22486-7), Coordenação de Aperfeiçoamento de Pessoal de Nível Superior (CAPES), Faculdade de Engenharia de Bauru (FEB/UNESP), Instituto de Física de São Carlos (IFSC/USP), Departamento de Física da Faculdade de Ciências (DF/UNESP), and Escola de Engenharia de São Carlos (EESC/USP).

References

Argawal, S., Rao, P.V., 2008. Experimental investigation of surface/subsurface damage formation and material removal mechanisms in SiC grinding. Int. J. Mach. Tools Manuf. 48 (6), 698–710.
Beyer, P., Ravenzwaaij, M., 2005. Innovative flat honing with vitrified-bond grinding and conditioning tools. Ind. Diamond Rev. IDR 4, 47–50.
Boch, P., Nièpce, J.C., 2007. Ceramic Materials: Processes Properties, and Applications, first ed. Wiley.
Brinksmeier, E., Mutlugünes, Y., Klocke, F., Aurich, L.C., Shore, P., Ohmori, H., 2010. Ultra-precision grinding. Ann. CIRP—Manuf. Technol. 59, 652–671.
Bukvic, G., Sanchez, L.E.A., Fortulan, C.A., Fiocchi, A.A., Marinescu, I.D., 2012. Green machining oriented to diminish density gradient for minimization of distortion in advanced ceramics. Mach. Sci. Technol. 16 (2), 228–246.
Burke, D.P., Rainforth, W.M., 1997. Intermediate rhombohedral phase formation at the surface of sintered Y-TZP. J. Mater. Sci. Lett. 16, 883–885.
Byrne, G., Dornfeld, D.A., Inasaki, I., Ketteler, G., Konig, W., Teti, R., 1995. Tool condition monitoring (TCM)—the status of research and industrial application. CIRP Ann.—Manuf. Technol. 44, 541–567.
Callister, W.D., Rethwisch, D.G., 2013. Materials Science and Engineering: An Introduction, ninth ed. Wiley.
Carvalho, R.C., 2007. Projeto de um mini-moinho vibratório auxiliado por técnicas de metodologia de projeto. 149f. In: Dissertação (Mestrado)—Escola de Engenharia de São Carlos. Universidade de São Paulo, São Carlos, 2010.
Carvalho, R.C., Fortulan, C.A., 2006. Projeto de um mini moinho vibratório auxiliado por técnicas de metodologia de projeto. Revista Minerva 3, 235–244.
Casellas, D., Cumbrera, F.L., Sánchez-Bajo, F., Forsling, W., Llanes, L., Anglada, M., 2001. On the transformation toughening of Y-ZrO_2 ceramics with mixed Y-TZP/PSZ microstructures. J. Eur. Ceram. Soc. 21 (6), 765–767.
Chevalier, J., Gremillard, L., Deville, S., 2007. Low-temperature degradation of zirconia and implications for biomedical implants. Annu. Rev. Mater. Res. 37, 1–32.
Clarke, D.R., Adar, F., 1982. Measurement of the crystallographically transformed zone produced by fracture in ceramics containing tetragonal zirconia. J. Am. Ceram. Soc. 65 (6), 284–288.
Deville, S., Chevalier, J., Gremillard, L., 2006. Influence of surface finish and residual stresses on the ageing sensitivity of biomedical grade zirconia. Biomaterials 27 (10), 2186–2192.
Fiocchi, A.A., 2010. Avanços no desenvolvimento de um processo de acabamento para peças planas submetidas à cinemática de lapidação sobre um rebolo dressado com grau de recobrimento. 143f. In: Dissertação (Mestrado)–Faculdade de Engenharia de Bauru. Universidade Estadual Paulista, Bauru.
Fiocchi, A.A., 2014. Ciência e tecnologia da manufatura de ultraprecisão de cerâmicas avançadas: Lapidorretificação Ud de superfícies planas de zircônia tetragonal policristalina estabilizada com ítria. 336f. In: Tese

(Doutorado)–Escola de Engenharia de São Carlos. Universidade de São Paulo, São Carlos, pp. 2014.
Fiocchi, A.A., Fortulan, C.A., Sanchez, L.E.A., 2015. Ultra-precision face grinding with constant pressure, lapping kinematics, and SiC grinding wheels dressed with overlap factor. Int. J. Adv. Manuf. Technol., http://dx.doi.org/10.1007/s00170-015-6933-5.
Fiocchi, A.A., Sanchez, L.E.A., Oliveira, J.F.G., Marinescu, I.D., 2011. Investigation on surface finishing of components ground with lapping kinematics: lapgrinding process. 13th CIRP Conference on Modeling of Machining Operations (CIRP CMMO,) Annals of the CIRP.
Flegler, A.J., Burye, T.E., Yang, Q., Nicholas, J.D., 2014. Cubic yttria stabilized zirconia sintering additive impacts: a comparative study. Ceram. Int. 40, 16323–16335.
Gatzen, H.H., Maetzig, J.C., 1997. Nanogrinding. Precis. Eng. 21, 134–139.
German, R.M., 1987. Theory of thermal debinding. Int. J. Powder Metall. 23 (4), 237–245.
Hasegawa, H., 1983. Rhombohedral phase produced in abraded surfaces of partially stabilized zirconia (PSZ). J. Mater. Sci. Lett. 2, 91–93.
Janssen, R., Scheppokat, S., Claussen, N., 2008. Tailor-made ceramic-based components—advantages by reactive processing and advanced shaping techniques. J. Eur. Ceram. Soc. 28 (7), 1369–1379.
Jemielniak, K., 1999. Commercial tool condition monitoring systems. Int. J. Adv. Manuf. Technol. 15 (10), 711–721.
Katagiri, G., Ishida, H., Ishitani, A., Masaki, T., 1988. Direct determination by Raman microprobe of the transformation zone size in Y_2O_3 containing tetragonal ZrO_2 polycrystals. In: Somiya, S., Yamamoto, N., Yanagida, H. (Eds.), Advances in Ceramics, Science and Technology of Zirconia III, 24. American Ceramic Society, Columbus, OH, pp. 537–544.
Kelly, P.M., Rose, L.R.F., 2002. The martensitic transformation in ceramics: its role in transformation toughening. Prog. Mater. Sci. 47 (5), 463–557.
Kerala, K., 2002. Machine design and drawing—II. Scheme and Syllabus. In: 2002–2003 Admission Onwards. Mahatma Gandhi University.
Kim, B., Hahn, J., Han, K.R., 1997. Quantitative phase analysis in tetragonal-rich tetragonal/monoclinic two phase zirconia by Raman spectroscopy. J. Mater. Sci. Lett. 16 (8), 669–671.
Kitano, Y., Mori, Y., Ishitani, A., Masaki, T., 1988. Rhombohedral phase in Y_2O_3 partially stabilized ZrO_2. J. Am. Ceram. Soc. 71 (1), C34–C36.
König, W., Messer, J., 1980. Dressing conventional grinding wheels with polycrystalline diamond (in German). Industrie-Anzeiger 102, 35–38.
Lai, L.J., Lu, H.C., Chen, H.K., Cheng, B.M., Lin, M.I., Chu, T.C., 2005. Photoluminescence of zirconia films with VUV excitation. J. Electron Spectrosc. Relat. Phenom. 144–147, 865–868.
Li, J., Zhang, L., Shen, Q., Hashida, T., 2001. Degradation of yttria stabilized zirconia at 370 K under a low applied stress. Mater. Sci. Eng. 297 (1–2), 26–30.
Lim, C.S., Finlayson, T.R., Ninio, F., Griffiths, J.R., 1992. In-situ measurement of the stress-induced phase transformation in magnesia-partially-stabilized zirconia using Raman spectroscopy. J. Am. Ceram. Soc. 75 (6), 1570–1573.
Malkin, S., 1989. Grinding technology: theory and applications of machining with abrasives, first ed. Chichester, Ellis Horwood Limited.
Malkin, S., Koren, Y., 1980. Off-line grinding optimization with a micro-computer. CIRP Ann. Manuf. Technol. 29 (1), 213–216.
Marinescu, I.D., Uhlmann, E., Doi, T., 2014. Handbook of Ceramics Grinding & Polishing, second ed. Elsevier.
Marinescu, I.D., Hitchiner, M., Uhlmann, E., Rowe, W.B., Inasaki, I., 2007. Handbook of Machining with Grinding Wheels. CRC Press, Wakefield.
Marinescu, I.D., Rowe, W.B., Dimitrov, B., Inasaki, I., 2004. Tribology of Abrasive Machining Processes, first ed. William Andrew Publishing, New York.
Marsh, D.M., 1964. Plastic flow in glass. Proc. R. Soc. Lond. A—Math. Phys. Eng. Sci. 279, 420–435.
Mehta, K., Jue, J.F., Virkar, A.V., 1990. Grinding-induced texture in ferroelastic tetragonal zirconia. J. Am. Ceram. Soc. 73 (6), 1777–1779.
Mitra, N., Vijayan, K., Pramila, B.N., Biswas, K., 1993. Phase transformation introduced by light mechanical and chemical surface preparation of tetragonal zirconia polycrystals. J. Am. Ceram. Soc. 76 (2), 533–535.
Ohmori, H., 2011. Ultrafine processing technology continues its evolution. Riken Res. 6 (11), 14–17.
Ohmori, H., Marinescu, I.D., Katahira, K., 2011. Electrolytic In-process Dressing (ELID) Technologies: Fundamentals and Applications, first ed. CRC Press.
Oliveira, J.F.G., Valente, C.M.O., 2004. Fast grinding process control with AE modulated power signals. CIRP Ann.—Manuf. Technol. 53 (1), 267–270.
Pahl, G., Beitz, W., Feldhusen, J., Grote, K.H., 2007. Engineering Design—A systematic Approach, third ed. Springer.
Pezzotti, G., Porporati, A.A., 2004. Raman spectroscopic analysis of phase-transformation and stress patterns in zirconia hip joints. J. Biomed. Opt. 9 (2), 372–384.
Richerson, D.W., 2006. Modern Ceramic Engineering: Properties, Processing, and Use in Design, third ed. CRC Press, New York.
Sanchez, L.E.A., Xu Jun, N.Z., Fiocchi, A.A., 2011. Surface finishing of flat pieces when submitted to lapping kinematics on abrasive disc dressed under several overlap factors. Precis. Eng. 35 (2), 355–363.
Sato, H., Yamada, K., Pezzotti, G., Nawa, M., Ban, S., 2008. Mechanical properties of dental zirconia ceramics changed with sandblasting and heat treatment. Dent. Mater. J. 27 (3), 408–414.
Scheller, W.L., 1994. Conventional machining of green aluminum/aluminum nitride ceramics. Ohio J. Sci. 94 (5), 151–154.
Schinker, M.G., Döll, W., 1987. Turning of optical glasses at room temperature. Proc. SPIE, Germany 802, 70–80.
Schmauder, S., Schubert, H., 1986. Significance of internal stresses for the martensitic transformation in yttria-stabilized tetragonal zirconia polycrystals during degradation. J. Am. Ceram. Soc. 69 (7), 534–540.
Sheng, G., Todd, R.I., 2011. Quantitative optical fluorescence microprobe measurements of stresses around indentations in Al_2O_3 and Al_2O_3/SiC nanocomposites: the influence of depth resolution and specimen translucency. Acta Mater. 59, 2637–2647.
Sikalidis, C., 2011. Advances in ceramics—characterization, raw materials, processing, properties, degradation and healing. In Tech.
Tabares, J.A.M., Anglada, M.J., 2010. Quantitative analysis of monoclinic phase in 3Y-TZP by Raman spectroscopy. J. Am. Ceram. Soc. 93 (6), 1790–1795.
Tabares, J.A.M., Piqué, E.J., Gasga, J.R., Anglada, M., 2011. Microstructural changes in ground 3Y-TZP and their effect on mechanical properties. Acta Mater. 59, 6670–6683.
Tomita, Y., Eda, H., 1996. A study of the ultra precision grinding process on a magnetic disk substrate - development of new bonding materials for fixed abrasives of grinding stone. Wear 195, 74–80.
Tönshoff, H.K., Friemuth, T., Becker, J.C., 2002. Process monitoring in grinding. CIRP Ann.—Manuf. Technol. 51 (2), 551–571.
Toraya, H., Yoshimura, M., Somiya, S., 1984a. Calibration curve for quantitative analysis of the monoclinic-tetragonal ZrO_2, system by X-ray diffraction. J. Am. Ceram. Soc. 67 (6), 119–121.
Toraya, H., Yoshimura, M., Somiya, S., 1984b. Quantitative analysis of monoclinic stabilized cubic ZrO_2 systems by X-ray diffraction. J. Am. Ceram. Soc. 67 (9), 183–184.
Virkar, A.V., Matsumoto, R.L.K., 1986. Ferroelastic domain switching as a toughening mechanism in tetragonal zirconia. J. Am. Ceram. Soc. 69 (10), 224–226.
Xu, H.H.K., Jahanmir, S., 1995. Effect of microstructure on abrasive machining of ceramics. Ceram. Eng. Sci. Proc. 16 (1), 295–314.
Xu, H.H.K., Padture, N.P., Jahanmir, S., 1995. Effect of microstructure on material-removal mechanisms and damage tolerance in abrasive machining of silicon carbide. J. Am. Ceram. Soc. 78 (9), 2443–2448.
Yoshimura, M., Noma, T., Kawabata, K., Somiya, S., 1987. Role of H_2O on the degradation process of Y-TZP. J. Mater. Sci. Lett. 6 (4), 465–467.
Zhuang, M., Wang, M., Zhao, Y., Zheng, B., Guo, A., Liu, J., 2015. Fabrication and high-temperature properties of Y-TZP ceramic helical springs by a gel-casting process. Ceram. Int. 41 (4), 5421–5428.

Arthur Alves Fiocchi studied Mechanical Engineering at the FEB/Unesp—Universidade Estadual Paulista (2007), has MSc in Mechanical Engineering from the same university (2010), and PhD in Mechanical Engineering at the EESC/USP—Universidade de São Paulo (2014). Substitute Professor at the Mechanical Engineering Department at FEB/Unesp from 2008 to 2011. He worked at General Motors Brazil at the Powertrain Division (2007). Manager and researcher of the Machining Technology Laboratory, LATUS, FEB/Unesp since 2007. Research/work experience in Canada, Germany, and USA. He has experience in Advanced Ceramics and Metals Manufacturing, especially characterization of such materials and design of ultra-precision machine-tools.

Luiz Eduardo de Angelo Sanchez studied Mechanical Engineer with graduation and PhD by Universidade de São Paulo EESC/USP, Brazil. Since 1993 works at the FEB/Unesp—Universidade Estadual Paulista, where develops studies about machining, mainly with focus on the improvement of tool-life and surface finish of metallic and ceramic workpieces through modifications in the traditional machining processes.

Paulo Lisboa-Filho studied Physics at the UFSCar—Universidade Federal de São Carlos (1996) and has a PhD in Sciences from the same university (2000). He was visiting researcher in Chimie du Solide et Matériaux at the Universitè Rennes I in France and since 2004 is Associate Professor of Physics at UNESP—Universidade Estadual Paulista in Bauru. He has experience in Condensed Matter Physics and Solid State Chemistry, especially in magnetic ceramics and biomaterials at the nanoscale.

Carlos Alberto Fortulan is Professor of Design in Mechanical Engineering. The main researches are related with: machine and tooling design for ceramics; design and manufacture of implants with functional gradient structure; direct manufacture of implants; design and manufacturing of ceramic membranes and design of orthoses and devices. Has started two Ceramic Industries in Brazil: Engecer Proj. e Prod. Cerâmicos S/A, 1985 and Cerauto Ind. E Com. Ltda, 1989. Member of the Ceramic Brazilian Association since 1987, Member Board of the Brazilian Center Ceramic (CCB) since 2009, and Parqtec (Technological Park) since 2002.